Chapter 3: Land use and land cover dynamics of Manas-Beki river basin

3.1 Introduction

Changes in land use and land cover (LULC) within the Manas-Beki river basin are analyzed in this chapter.

The following aspects are included to understand the overall changes in the basin:

i. LULC changes in the areas adjacent to the river in the floodplain region from 1990 to 2020.
ii. Vegetation and snow cover changes in the upper glaciated catchments from 1990 to 2020.

The causes and consequences of LULC change have been widely studied by researchers because of its linkage to ecosystem dynamics, resource management, food security, climate change, and an array of other biophysical processes and phenomena [1, 2, 3].

Land cover dynamics within a river basin is governed by both natural and anthropogenic factors and its study is integral to understand the changes in the hydrogeomorphology of a river [4]. LULC changes can impact the hydro-geomorphological regime of drainage basins [5, 6]. Drainage basins are sensitive to changes in the LULC affecting the stream runoff, sediment supply, and overall water availability with an increased potentiality of occurrence of extreme events such as floods and droughts [7 – 12].

The major drivers of land use change are attributed to human causes including deforestation, agricultural intensification, and urbanization whereas land cover changes are primarily linked to changes in the climate or the occurrence of extreme events such as floods, droughts, landslides, earthquakes, forest fires, and related natural disasters. [13 – 18].

In the floodplains, the influence of human activities is more pronounced and changes in LULC can impact the highly unstable fluvial environment [19, 20]. Improper land utilization of floodplains can result in changes in the river's morphology, bank instability resulting in erosion/accretion, changes in sediment dynamics, and increased flood risks among others [21 – 25]. On the other hand, LULC changes can also be driven by fluvial dynamics, especially in the young and extremely active rivers originating in the Himalayas [26] and by frequent flooding [1]. It is important to understand the LULC and its changes in the river corridor for water resource management and sustainable management of resources available in the

floodplains [27, 28, 29]. The Brahmaputra floodplains are characterized by rapid changes in fluvial characteristics resulting in changes in the LULC [26, 30].

In glaciated basins, the impact of land cover changes at higher elevations, including changes in natural vegetation and snow/ice-covered areas, on the hydrological regime of the river can be immense. Glacier changes impact surface runoff and forest changes can significantly alter evapotranspiration and soil moisture, thus LULC change analysis is a crucial input to understand the hydrological implications of climate change [31]. LULC changes in the upper reaches help to understand the dynamics of water availability and flood regimes in the downstream areas [32, 33]. Land cover changes such as increase in vegetation cover is linked to decrease in runoff [34, 35], whereas decrease in snow cover and glacier extents is linked to increased streamflow [36, 37, 38]. The Himalayas is likely to be particularly vulnerable to observed changes in the climate with notable changes in the extent of vegetation and snow cover [39 – 42]. Limited studies on land cover changes in the Bhutan Himalayas also provide similar insights to an increase in vegetation cover and a decrease in snow cover [43, 44]. With the impacts of global climate change evident in almost all ecosystems, it is important to analyze the LULC changes at the basin level to understand its possible repercussions.

In this chapter, the changes in land use and land cover is quantified for three decades (1990 – 2020), with emphasis on the active floodplain river corridor and the glaciated upper catchments.

3.2 Data and methods

3.2.1 Data and resources used

Geospatial data and methods were used to develop LULC maps for the area adjacent to the river in the floodplains as well as detect changes in vegetation and snow in the upper catchments. Satellite images of four different time periods, 1990, 2000, 2010, and 2020, were used to extract land use and land cover information of the Manas-Beki basin. Landsat images obtained from USGS of similar spatial resolution were identified for the study. The details of the dataset used for the study is presented in Table 3.1.

Erdas Imagine software was used for classification and post-classification analysis and ArcGIS software was used for mapping and statistical analysis. Google Earth Engine (GEE), which is an open-source cloud-based platform for geospatial data analysis and visualization, was used for analyzing the seasonal changes in snow cover from 1990 to 2020.

Table 3.1 Details of satellite data used for LULC change analysis in Manas-Beki basin, 1990-2020

Satellite/ sensors	Spatial resolution	Time of acquisition	Path	Row	No. of scenes	Source
Landsat TM	30 m	Nov/Dec 1990	137	40-42	3	USGS
Landsat TM	30 m	Nov/Dec 1990	138	41-42	2	USGS
Landsat ETM+	30 m	Nov/Dec 2000	137	40-42	3	USGS
Landsat ETM+	30 m	Nov/Dec 2000	138	41-42	2	USGS
Landsat TM	30 m	Nov/Dec 2010	137	40-42	3	USGS
Landsat TM	30 m	Nov/Dec 2010	138	41-42	2	USGS
Landsat OLI	30 m	Nov/Dec 2020	137	40-42	3	USGS
Landsat OLI	30 m	Nov/Dec 2020	138	41-42	2	USGS

3.2.2 Methodology

The schema of overall methodology used for LULC classifications and change analysis in the floodplains, vegetation, and snow cover extraction and change in the upper catchments and analysis of seasonal snow cover changes in the Manas-Beki river basin is presented in Figure 3.1. The detailed methodology is explained in the following sub-sections.

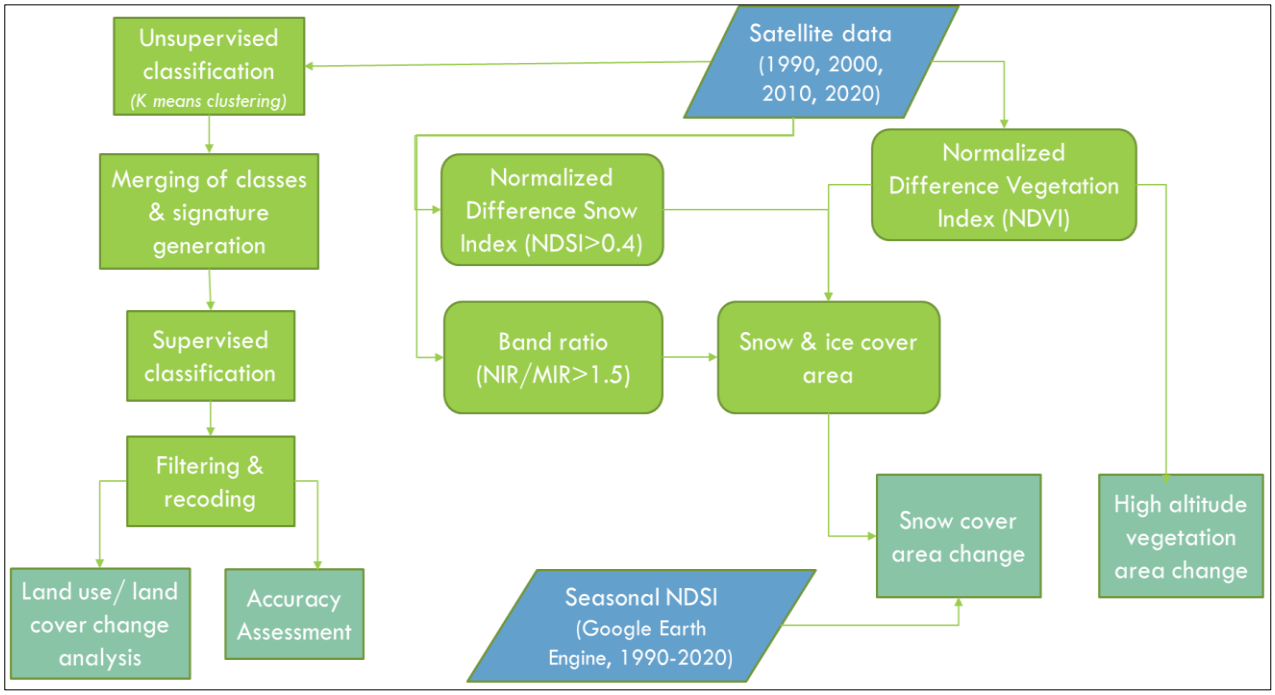

Figure 3.1 Flowchart of overall methodology used for land use and land cover classification and change analysis

To work out the land classes to be included in the final study, a preliminary analysis was carried out using LULC dataset available from the North Eastern Space Applications Centre (NESAC), Govt. of India. This dataset (from NESAC) is for the part of the Manas-Beki basin falling within the jurisdiction of India and is at the scale of 1:50,000 for the period 2015-16. For the area falling outside India, Landsat (OLI) data of 2016 was used. The classification was done for the broad Level 1 classes in the NESAC classification using a visual interpretation method to be comparable to the NESAC dataset. A composite LULC map for the entire basin was prepared to understand the overall LULC. A total of 12 classes were available for the basin including Dense Forest, Open Forest, Scrublands, Grassland, Ice/Snow, Barren Land, Tree Clad Area, Agriculture, Settlement, Waterbodies, Streams/rivers, and Wetlands. The percentage of areas within each class was analyzed (Figure 3.2) and it was observed that the highest area was covered by the forest classes (dense and open forest) which together constituted almost 46% of the basin followed by snow- and ice-covered area (~26%). The other major classes were scrublands (~8.5%), agricultural area (~8%), barren land (~6%), tree clad area (~2%), and area of streams or rivers (~2%). It was observed that the forest, snow, and barren area composed almost 95% of the total area in the upper catchments of Mangde, Chamkar, Kuri and Dangme, and the other classes were mainly seen in the floodplain region. Therefore, the LULC change analysis was studied separately for both the floodplain and the upper catchment areas. Since the impact of land use in the upper catchment was negligible compared to the natural vegetation and snow-covered areas, therefore only these two aspects were analyzed. In the floodplain region, LULC changes were observed from 1990-2020 for the areas adjoining the river to understand the influence of river changes on LULC.

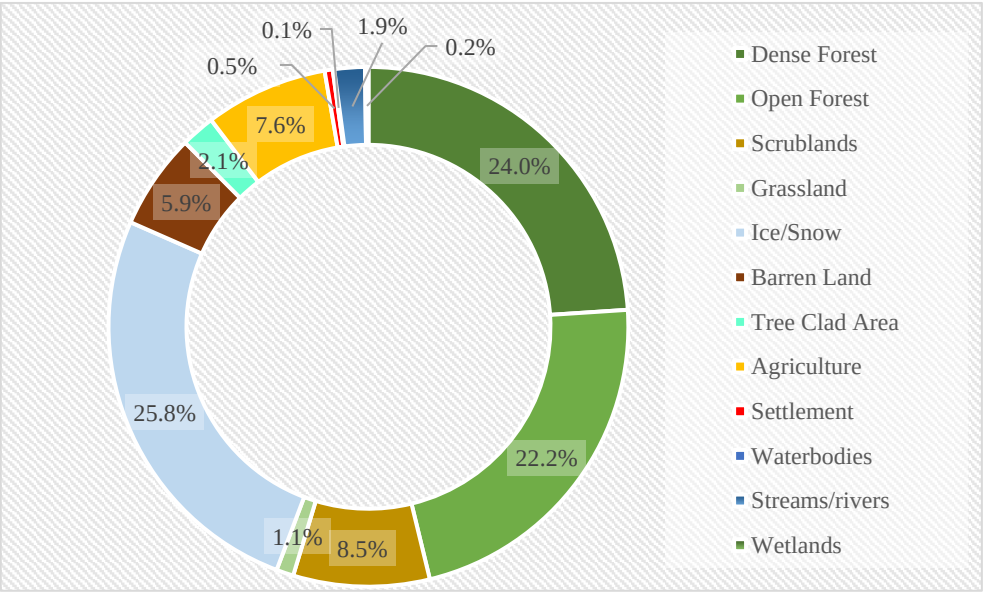

Figure 3.2 LULC classes in the Manas-Beki river basin

Land use classification and change analysis in the floodplains

The river channel from 1990 to 2020 was merged and the maximum area coverage was used to identify the areas 5 km surrounding the maximum coverage. A total area of approximately 1225 km^2 in the floodplains was demarcated for LULC change analysis. The Landsat images with path/row 137/42 of 1990, 2000, 2010, and 2020 were used for extracting this floodplain region. For proper identification of land cover features basic image pre-processing is imperative. Radiometric normalization was carried out for multi-date and multi-sensor satellite data. Normalization reduces inconsistencies in the satellite images which are inherent in the images because of differences in acquisition conditions such as variation in sun zenith angles, shadow effect, sensor calibrations, and atmospheric conditions, etc. [45, 46]. In radiometric corrections, haze reduction, noise reduction, and histogram equalization were performed for all the satellite images in the Erdas Imagine software. It is important to have the images from different time periods perfectly aligned at the pixel level for change detection studies [47]. Even though Landsat images are pre-aligned to each other, image-to-image calibration was carried out in the Autosync module of Erdas Imagine software to ensure that all four images were aligned to each other with less than half pixel accuracy.

Hybrid classification, which is a combination of unsupervised and supervised digital classification [26] was performed for classifying the area into 6 distinct classes representative of the region. The 6 classes identified for LULC change analysis are water bodies, vegetation, grassland, agriculture sand, and settlement. The classification scheme used for the present study has been modified from Hazarika et al. and the description of each class is given in Table 3.2 [26]. These classes are broadly representing the LULC of the study area and can be easily determined by moderate resolution of Landsat imagery.

Table 3.2 LULC classes adopted for change analysis in Manas-Beki basin

LULC Code	LULC Class	Description
1	Water bodies	Open water features such as rivers, streams, lakes, and reservoirs. Low-lying areas saturated with moisture and covered with aquatic vegetation such as water hyacinth.
2	Vegetation	It included areas under dense, open forests, scrublands, plantations like orchards and tea gardens, and rural built-up with homestead land.

3	Grassland	Areas dominated by grasses including vegetated sandbars and grazing areas
4	Agriculture	Areas under cultivation including current fallow areas
5	Sand	Sandbars and other sand deposition areas including both dry and wet sand areas.
6	Settlement	Areas under urban built-up including roads and other concrete areas

The images for each year were first classified by an unsupervised method which uses the reflectance value of the pixels to cluster into different groups based on statistical patterns of values. These are simply clusters of pixels with similar spectral characteristics and must be interpreted into meaningful classes of interest [48]. The ISODATA unsupervised classification algorithm [49] was used to automatically classify the satellite images of the study area into 36 classes with similar spectral characteristics. These classes were then merged into the six information classes based on the classification scheme adopted for the study. Signatures are then generated for these six classes which are used to reclassify the original satellite images using Maximum Likelihood Classifier which is a supervised classification method. The final classified images were then filtered using a neighbourhood majority function with the help of a 3×3 matrix window which replaces the central pixel in the matrix with the most common data file value in the window. This is required for the removal of noise, reduction of the salt and pepper effect, and smoothening of classes in the classified images. Recoding was performed for major misclassification of features with similar spectral characteristics such as water-shadow and sand-settlement.

The accuracy of each classified image was assessed by a set of 120 random points based on the number of classes (20 points per class). Examination of satellite images and high-resolution images from Google Earth were used for assigning reference classes. Field verifications were carried out in 2020 and the points were used as reference for checking the accuracy of the LULC map developed for 2020. For each map, a confusion matrix or error matrix was created with each row representing land-use classes in the classified map and each column representing the reference land-use classes. The overall accuracy and Kappa analysis were used to perform classification accuracy assessment based on error matrix analysis. The overall accuracy is calculated by summing the number of pixels classified correctly and dividing by the total number of pixels. Kappa analysis is a discrete multivariate technique of use in accuracy

assessment [50]. It is the degree of correctness between the classified map and the reference map. User's accuracy and producer's accuracy were also calculated. User's accuracy measures the proportion of each class which is correctly classified in the map as a particular class and producer's accuracy measures the proportion of land use class which is correctly classified as the actual landscape present on the ground. Kappa co-efficient is measured by using the following formula [51]:

$$K = \frac{\mathrm{N(Xii) - (Xi+) - (Xi + \times X + i)}}{\mathrm{N(Xi+) - (Xi + \times X + i)}}$$

where X_{ii} is the number of observations correctly classified for a particular category, X_{i+} and X_{+i} are the marginal totals for row i and column i associated with the category, and N is the total number of observations in the entire error matrix.

The final classified images were used to generate land use and land cover statistics for the entire study area for 1990, 2000, 2010, and 2020. Post-classification change detection was carried out by developing the change matrix between different years of analysis, 1990-2000, 2000-2010, and 2010-2020. Post-classification analysis of change using transition matrices is a reliable method of quantifying changes between classes between different time periods [1, 52]. The classification and generation of change matrices were done using Erdas Imagine, mapping in ArcGIS, and area statistics were analyzed in Microsoft Excel software.

Land cover changes in the upper glaciated catchments

The upper glaciated catchments of Dangme Chu, Kuri Chu, Chamkar Chu, and Mangde Chu from east to west were observed for changes in vegetation and snow cover from 1990 to 2020. Landsat images from 1990, 2000, 2010, and 2020 were used (Figure 3.3) and the combined area for all four catchments (~28,512 km^2) as well as individual catchments were studied separately.

To analyze the changes in vegetation in the upper catchments, the Normalized Difference Vegetation Index (NDVI) was used. NDVI has been used by many researchers to identify vegetated areas and analyze changes in vegetation [53, 54, 55]. NDVI is calculated using reflectance values for the Red and Infrared wavelengths of the spectrum as given in the following formula: NDVI = (Near Infrared – Red)/ (Near Infrared + Red). For Landsat TM and ETM sensors, NDVI calculation requires information from Band 3 (Red) and Band 4 (NIR) while for the Landsat OLI sensor, Band 4 (Red) and Band 5 (NIR) are required. NDVI is a

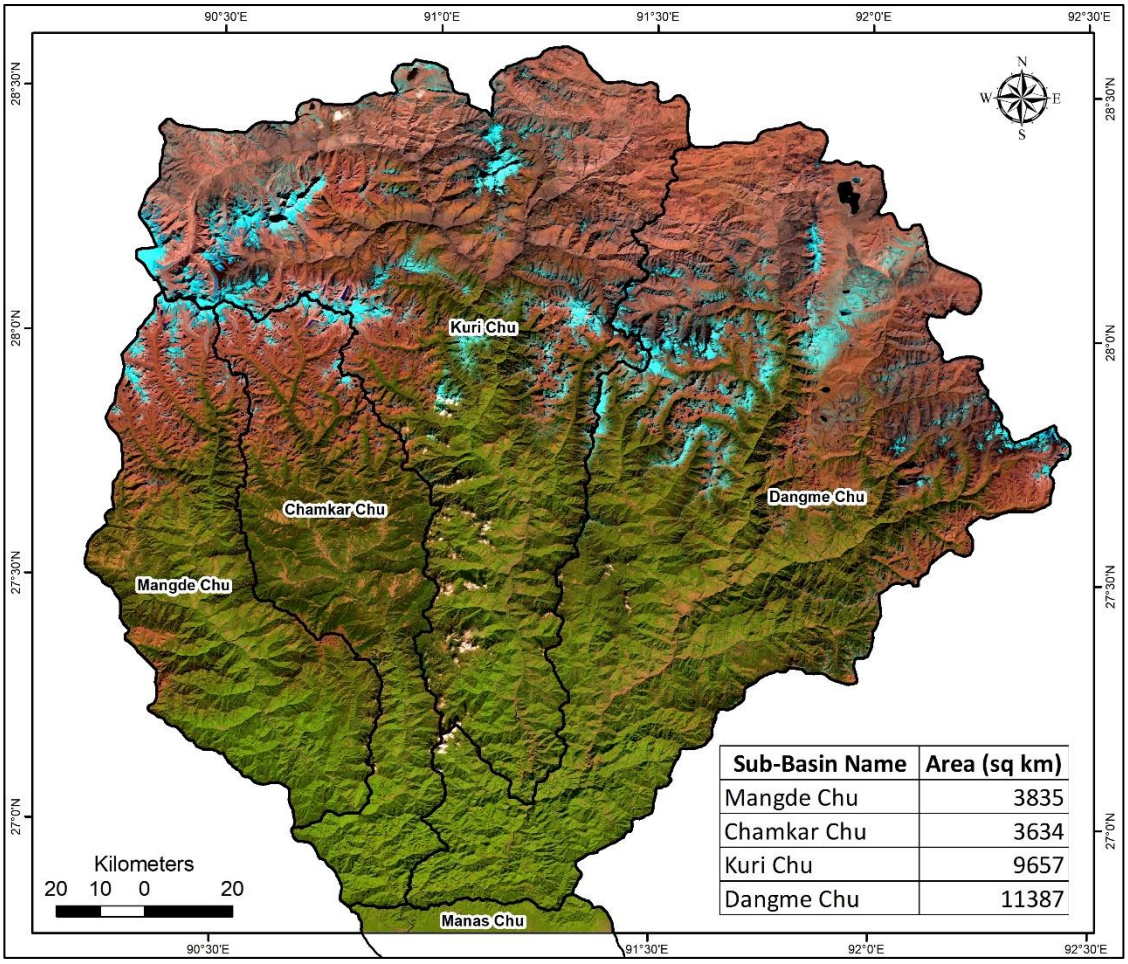

Figure 3.3 Glaciated upper catchments as visualized in Landsat 8 False Colour Composite (Band 7, 4 and 3) with their areas for vegetation and snow cover analysis

direct indicator of vegetation health, and the values range from -1 to +1, with higher values indicating healthy and dense vegetation. NDVI was calculated for each satellite image year-wise composite from 1990 and 2020. The image statistics were analyzed for each image and the NDVI difference image was calculated to visualize the areas of overall change between 1990 to 2020.

The areas with no change were the areas with values around 0 and thresholds were used to classify the NDVI difference images into three classes based on standard deviation (SD) from mean: No change (-1 to +1 SD), negative change (< -1 SD) and positive change (>1 SD) [54, 56].

At higher altitudes, the demarcation between vegetation and barren land is distinct, and it was possible to extract vegetation areas based on NDVI values. Image thresholding was carried out to separate the vegetation areas based on manual checking of values against each satellite composite based on visual observation of satellite images [57, 58]. The thresholds for

vegetation extraction varied between 0.4 and 0.5 for each image composite of the study area. The final vegetation maps for 1990, 2000, 2010, and 2020 were prepared after noise removal using majority filters. Since the satellite data were radiometrically normalized and images were used for the same time of the year (December), the vegetation areas extracted for each year and sub-basin were compared for change analysis.

Spectral indices including Normalized Difference Snow Index (NDSI), NDVI, band ratio of NIR, and Mid-Infrared (MIR) data along with elevation information for the glaciated sub-basins under Manas-Beki basin were used to estimate snow and ice cover areas from Landsat satellite images for 1990, 2000, 2010 and 2020. The methodology was based on Racoviteanu *et al* and the criteria used for the extraction of snow and ice areas are given in Table 3.3 [58]. Snow cover maps were prepared for the same time (December) of each year and area changes were estimated for each catchment.

Table 3.3 Criteria used for extraction of snow and ice-covered areas in Manas-Beki basin

Criteria	Formula	Condition applied
Normalized Difference Vegetation Index (NDVI)	(NIR – Red)/(NIR + Red)	<0.2
Normalized Difference Snow Index (NDSI)	(Green – SWIR)/(Green + SWIR)	>0.4
Band ratio	NIR/MIR	>1.5
Elevation	-	>3000 m

Google Earth Engine (GEE), which is an open-source platform for cloud-based geospatial analysis, was used to calculate NDSI values for each season from 1990 to 2020 to understand the seasonal changes. Four seasons were considered based on months, viz. Jan-Mar, Apr-Jun, Jul-Sep and Oct-Dec. Landsat daily NDSI composites for the entire study area were generated using the maximum function to extract maximum snow cover during the identified seasons. A threshold of 0.4 was used to extract snow cover areas from NDSI output and annual seasonal data was downloaded for further analysis. GEE was also used to download monthly ERA5 reanalysis data for snow cover for the four catchments, to compare results derived from NDSI. The extracted vegetation and snow areas were also analyzed at each elevation zone based on DEM data to check any trends at different elevations.

3.3 Results

3.3.1 Land use classification and change analysis in the floodplains

The areas associated within a 5 km distance from the river courses from 1990 to 2020 in the floodplain region in Assam were classified using hybrid classification method into six classes: Water bodies, Vegetation, Grassland, Agriculture, Sand, and Settlement followed by noise removal and recoding for misclassified classes. Accuracy assessment of the classified images using 120 random points show overall accuracies of 86.67%, 87.5%, 87.5%, and 92.5%; and kappa coefficient of agreement of 0.84, 0.85, 0.85, and 0.91 for 1990, 2000, 2010 and 2020 respectively (Table 3.4a – 3.4d). In terms of producer's accuracy or user's accuracy, all classes were between 68% and 100%. Mostly the grassland and agriculture classes were wrongly classified. The classified images show relatively high accuracies making them eligible for change detection studies.

The final classified maps for 1990, 2000, 2010, and 2020 after filtering and recoding are shown in Figures 3.4a, 3.4b, 3.4c, and 3.4d respectively and pie diagrams showing the percentage of area under each land use and land cover category are shown in Figures 3.5a, 3.5b, 3.5c and 3.5d. All the years show agriculture as the most dominant land use type. Vegetation classes (comprising forests, plantations, and other trees) cover the second highest area followed by grasslands. Settlement class covers the least area, but is increasing from 1990 to 2020.

Change analysis shows highly dynamic results through the years (Table 3.5). Water areas have decreased between 1990-2000 and 2000-2010 but increased during 2010-2020. Vegetation areas including forests and other tree-clad areas have decreased between 1990-2000 but increased in the other two decades. Grassland areas decreased between 1990-2000 but increased during 2000-2010 and 2010-2020. Agriculture areas show an increase between 1990-2000 but decrease thereafter. Sand deposition areas show a large increase in area (~49 km^2) but decrease by around 37 km^2 during 2010-2020. The area changes under different LULC categories during 1990-2020 are shown in Figure 3.6.

Table 3.4a Confusion matrix for hybrid classification of Manas-Beki floodplain region, 1990

LULC classes	Water	Vegetation	Grassland	Agriculture	Sand	Settlement	Reference total	Producer's accuracy	User's accuracy
Water	19		1				20	95.00%	95.00%
Vegetation		16	2	2			20	88.89%	80.00%
Grassland	1		15	4			20	83.33%	75.00%
Agriculture				19	1		20	67.86%	95.00%
Sand				3	17		20	94.44%	85.00%
Settlement		2				18	20	100.00%	90.00%
Total	20	18	18	28	18	18	120		
Overall classification accuracy			**86.67%**		**Kappa co-efficient**		**0.84**		

Table 3.4b Confusion matrix for hybrid classification of Manas-Beki floodplain region, 2000

LULC classes	Water	Vegetation	Grassland	Agriculture	Sand	Settlement	Reference total	Producer's accuracy	User's accuracy
Water	19			1			20	90.48%	95.00%
Vegetation		17	3				20	89.47%	85.00%
Grassland			16	3	1		20	80.00%	80.00%
Agriculture				20			20	76.92%	100.00%
Sand	1		1	1	17		20	94.44%	85.00%
Settlement	1	2		1		16	20	100.00%	80.00%
Total	21	19	20	26	18	16	120		
Overall classification accuracy			**87.50%**		**Kappa co-efficient**		**0.85**		

Table 3.4c Confusion matrix for hybrid classification of Manas-Beki floodplain region, 2010

LULC classes	Water	Vegetation	Grassland	Agriculture	Sand	Settlement	Reference total	Producer's accuracy	User's accuracy
Water	19				1		20	86.36%	95.00%
Vegetation		16	3	1			20	88.89%	80.00%
Grassland	2		16	2			20	80.00%	80.00%
Agriculture			1	18	1		20	81.82%	90.00%
Sand	1			1	18		20	90.00%	90.00%
Settlement		2				18	20	100.00%	90.00%
Total	22	18	20	22	20	18	120		
Overall classification accuracy			**87.50%**		**Kappa co-efficient**		**0.85**		

Table 3.4d Confusion matrix for hybrid classification of Manas-Beki floodplain region, 2020

LULC classes	Water	Vegetation	Grassland	Agriculture	Sand	Settlement	Reference total	Producer's accuracy	User's accuracy
Water	20						20	90.91%	100.00%
Vegetation		19	1				20	100.00%	95.00%
Grassland	1		16	2	1		20	94.12%	80.00%
Agriculture	1			17	1	1	20	85.00%	85.00%
Sand					20		20	90.91%	100.00%
Settlement				1		19	20	95.00%	95.00%
Total	22	19	17	20	22	20	120		
Overall classification accuracy			**92.50%**		**Kappa co-efficient**		**0.91**		

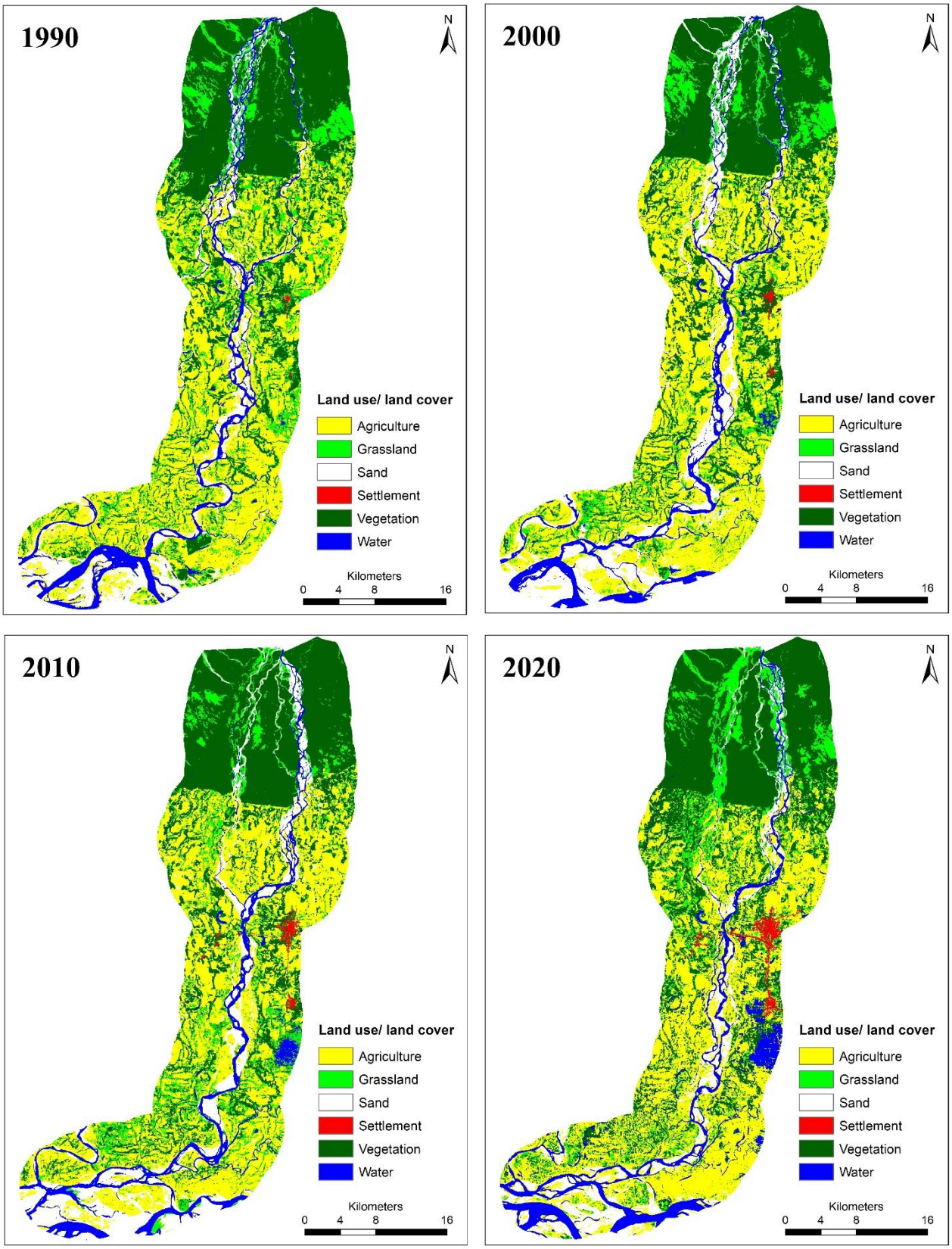

Figure 3.4 LULC in the Manas-Beki floodplain region for (a) 1990, (b) 2000, (c) 2010 and (d) 2020

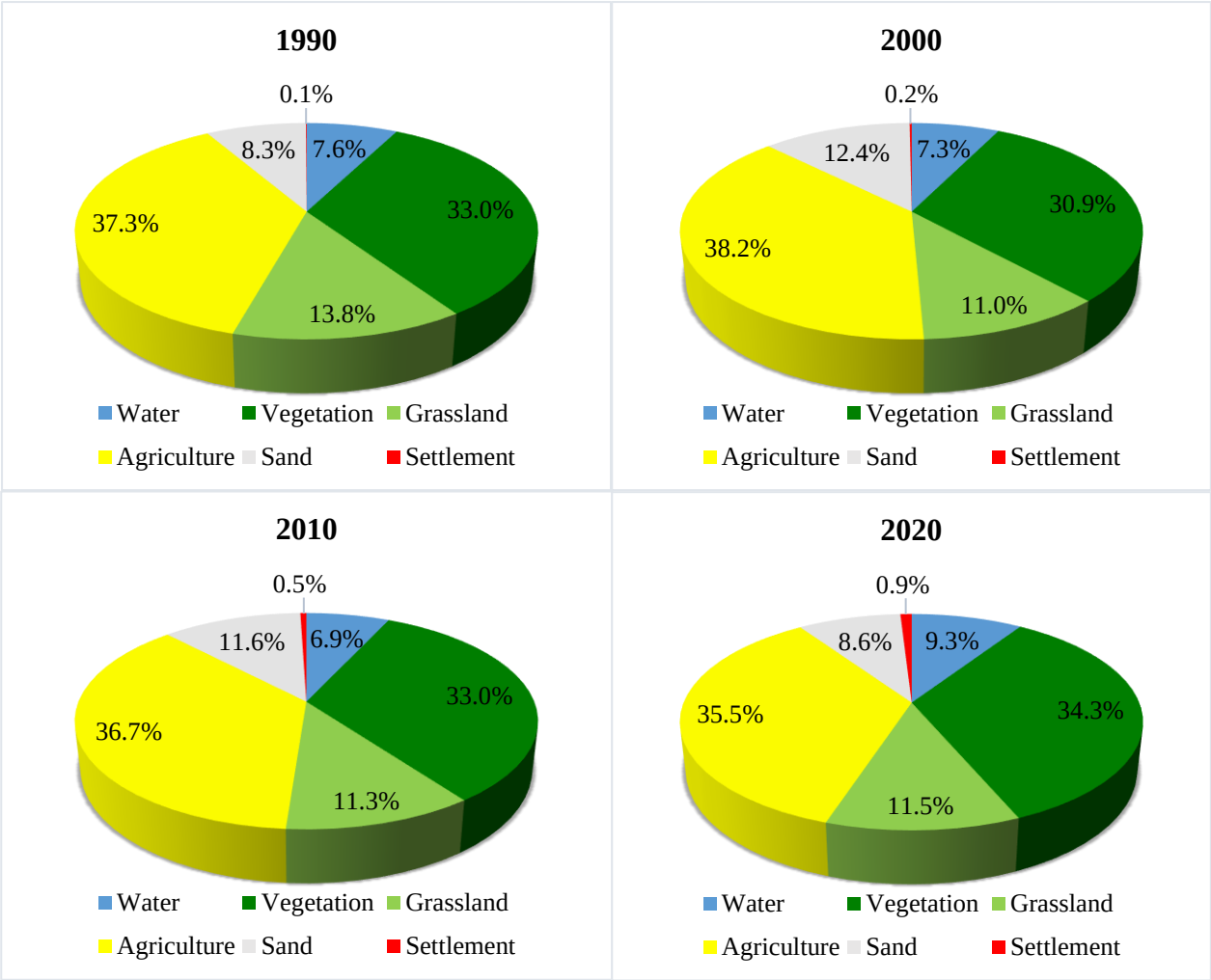

Figure 3.5 Percentage areas under different LULC categories for 1990, 2000, 2010 and 2020 in Manas-Beki floodplains

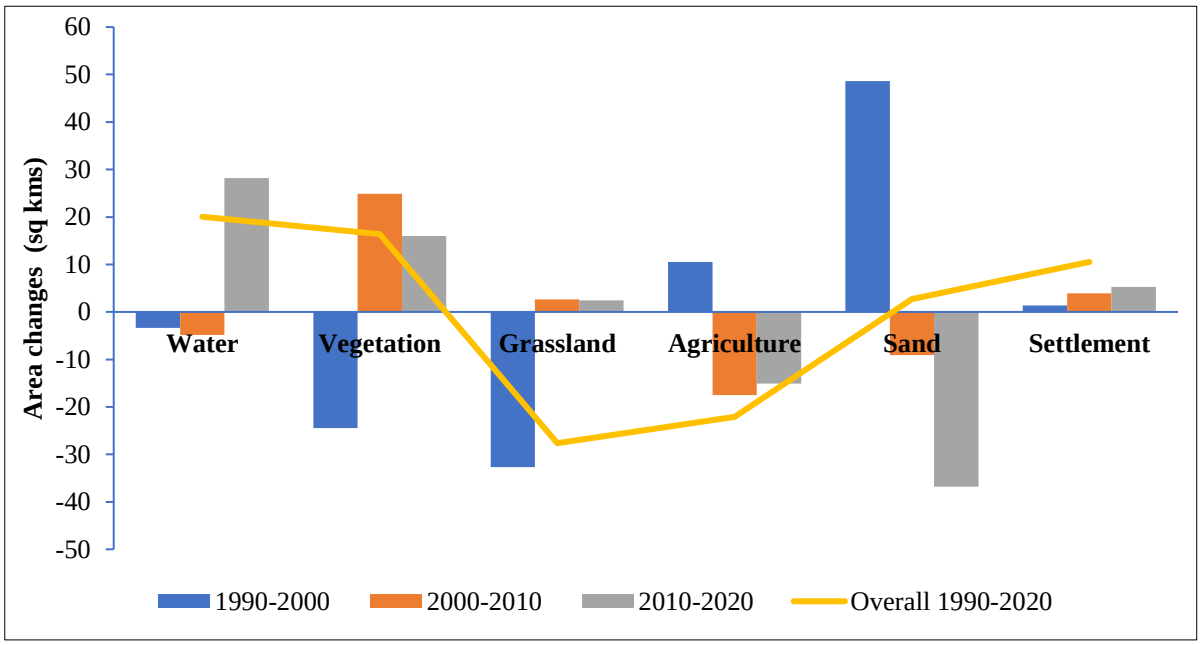

Figure 3.6 Area change in LULC categories in Manas-Beki floodplains, 1990-2020
(Positive change indicate gain and negative change indicate loss)

Table 3.5 LULC statistics in the floodplains of Manas-Beki river during 1990, 2000, 2010 and 2020

LULC Code	LULC class	Area (ha)				Area Change (ha)			Net area change (ha)
		1990	2000	2010	2020	1990-2000	2000-2010	2010-2020	1990-2020
1	Water	9145.53	8812.26	8328.78	11150.20	-333.27	-483.48	2821.42	2004.67
2	Vegetation	39707.60	37259.40	39745.20	41344.00	-2448.20	2485.80	1598.80	1636.40
3	Grassland	16577.60	13307.90	13572.60	13813.60	-3269.70	264.70	241.00	-2764.00
4	Agriculture	44921.40	45972.00	44217.30	42710.80	1050.60	-1754.70	-1506.50	-2210.60
5	Sand	10034.00	14897.90	13989.40	10306.70	4863.90	-908.50	-3682.70	272.70
6	Settlement	72.36	205.65	597.60	1126.17	133.29	391.95	528.57	1053.81

(Negative values indicate decrease in area and positive values indicate increase in area for LULC area changes)

LULC changes were quantified between the years by developing the change matrix for each period. Tables 3.6(a), 3.6(b), and 3.6 (c) show the change matrix tables generated for 1990-2000, 2000-2010, and 2010-2020 respectively. The tables depict the highly variable nature of LULC within the floodplain with notable changes in each period. The highlighted values indicate the unchanged areas which is varying from as low as 25% for grasslands to 87% for settlement areas during 1990-2000. It varies between 27% for grasslands to 82% for vegetation areas between 2000 to 2010 and between 24% for grasslands to 79% for settlement and vegetation areas. This shows that grasslands are the most variable LULC class within the area of analysis.

Table 3.6a Change matrix of LULC classes in floodplain of Manas-Beki river, 1990-2000

1990 (Area in ha)	**2000 (Area in ha)**						
Classes	Water	Vegetation	Grassland	Agriculture	Sand	Settlement	Total
Water	2600	246	432	1484	4382		9144
Vegetation	844	30786	3567	3559	895	47	39697
Grassland	818	3859	4182	6397	1256	58	16570
Agriculture	2265	2153	4595	31760	4095	37	44905
Sand	2280	200	527	2755	4269		10031
Settlement	1	7		1		63	72
Total	8808	37251	13303	45956	14896	205	120419

Table 3.6b Change matrix of LULC classes in floodplain of Manas-Beki river, 2000-2010

2000 (Area in ha)	**2010 (Area in ha)**						
Classes	Water	Vegetation	Grassland	Agriculture	Sand	Settlement	Total
Water	2575	530	736	1341	3622	8	8811
Vegetation	749	30540	2782	2012	906	264	37253
Grassland	592	4786	3569	3689	621	44	13302
Agriculture	2102	2706	5040	32394	3592	118	45952
Sand	2308	1157	1426	4759	5245		14895
Settlement		17	15	10		163	205
Total	8327	39735	13568	44204	13986	597	120418

Table 3.6c Change matrix of LULC classes in floodplain of Manas-Beki river, 2010-2020

2010 (Area in ha)	**2020 (Area in ha)**						
Classes	Water	Vegetation	Grassland	Agriculture	Sand	Settlement	Total
Water	3448	178	320	1814	2562	5	8327
Vegetation	705	31480	3003	4093	248	208	39736
Grassland	1322	3605	3210	4866	423	142	13567
Agriculture	1896	5770	5700	28263	2274	299	44202
Sand	3776	272	1557	3583	4797	1	13985
Settlement	1	27	20	76		472	598
Total	11148	41332	13810	42695	10305	1126	120415

The LULC categories were also analyzed for the areas which were affected by fluvial dynamics from 1990 to 2020. The LULC classes affected due to changes in river morphology were analyzed and areas within each class that were lost due to erosion or gained due to deposition were estimated (Table 3.7). Changes in the settlement class were negligible and not included in the analysis. Changes in vegetation, grassland, and sand categories can be related to the erosional and depositional processes of the river due to channel changes while agriculture area changes do not show any relation. The LULC areas affected by erosion and deposition from 1990 to 2020 are shown in Figure 3.7.

Table 3.7 LULC classes in Manas-Beki floodplain affected by erosion and deposition during 1990-2020

LULC Code	LULC Class	Erosion (km^2)			Deposition (km^2)		
		1990-2000	2000-2010	2010-2020	1990-2000	2000-2010	2010-2020
1	Water	4.4	1.6	0.4	4.8	0.5	0.7
2	Vegetation	33.7	9.2	3.2	2.9	10.1	3.2
3	Grassland	8.8	3.6	1.9	4.6	9.0	6.6
4	Agriculture	25.6	22.5	10.0	14.7	22.8	14.7
5	Sand	3.2	4.8	1.1	16.6	1.2	3.0

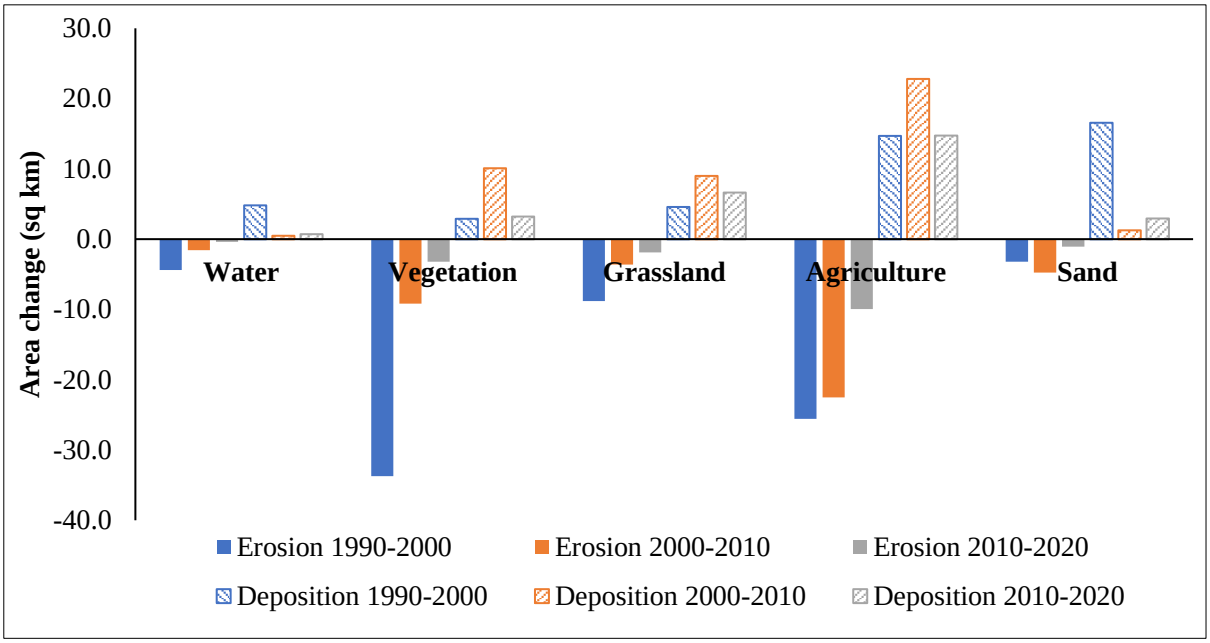

Figure 3.7 Area change in LULC categories due to erosion and deposition in Manas-Beki floodplains, 1990-2020
(Positive change indicate deposition and negative change indicate erosion)

3.3.2 Vegetation cover changes in the upper catchments

The Landsat composites for each year, 1990, 2000, 2010, and 2020 were used to estimate NDVI values for the area within the four glaciated sub-basins: Mangde Chu, Chamkar Chu, Kuri Chu, and Dangme Chu from the west to east of Manas-Beki basin. The statistics for each of these NDVI images were generated including minimum/ maximum values, range, mean, median, and standard deviation. The mean values for each sub-basin as well as all the four sub-basins together are given in Table 3.7. The values do not show considerable changes from 1990 to 2010 with a slight decreasing trend but the values have increased for 2020 for all the catchments (Figure 3.8). The highest difference is observed in the westernmost sub-basin of Mangde Chu.

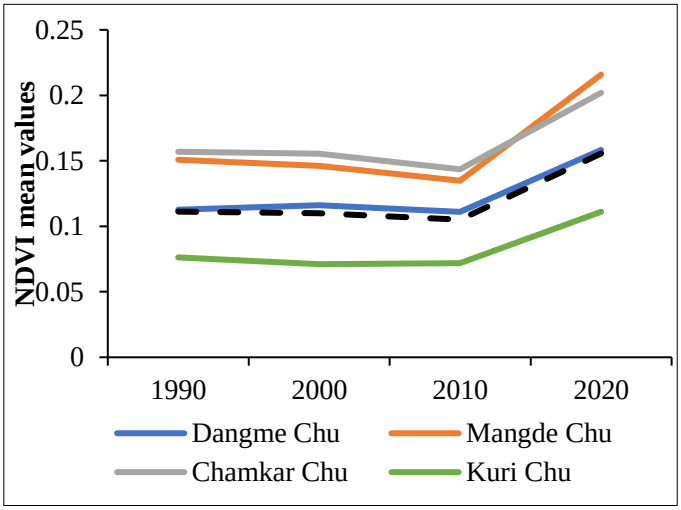

Figure 3.8 Mean NDVI values for each sub-basin in Manas-Beki basin (1990-2020)

Table 3.8 Mean NDVI values for different sub-basins in Manas-Beki basin (1990-2020)

Sub-basin	Mean NDVI values			
	1990	**2000**	**2010**	**2020**
Dangme Chu	0.113	0.116	0.111	0.158
Mangde Chu	0.151	0.146	0.135	0.216
Chamkar Chu	0.157	0.156	0.144	0.202
Kuri Chu	0.076	0.071	0.072	0.111
Overall	0.111	0.110	0.105	0.156

NDVI difference image was calculated to visualize the areas of overall change between 1990 to 2020 and classified into three classes (no change, positive change, and negative change) based on 1 standard deviation values (Figure 3.9). The NDVI difference image shows that the NDVI values have increased in the low-vegetated areas while it has decreased in the upper barren land region. The highest area with a positive change is in the Mangde Chu basin (~48%), followed by Chamkar Chu and Dangme Chu (~28.5%), and the least change in Kuri Chu (19%).

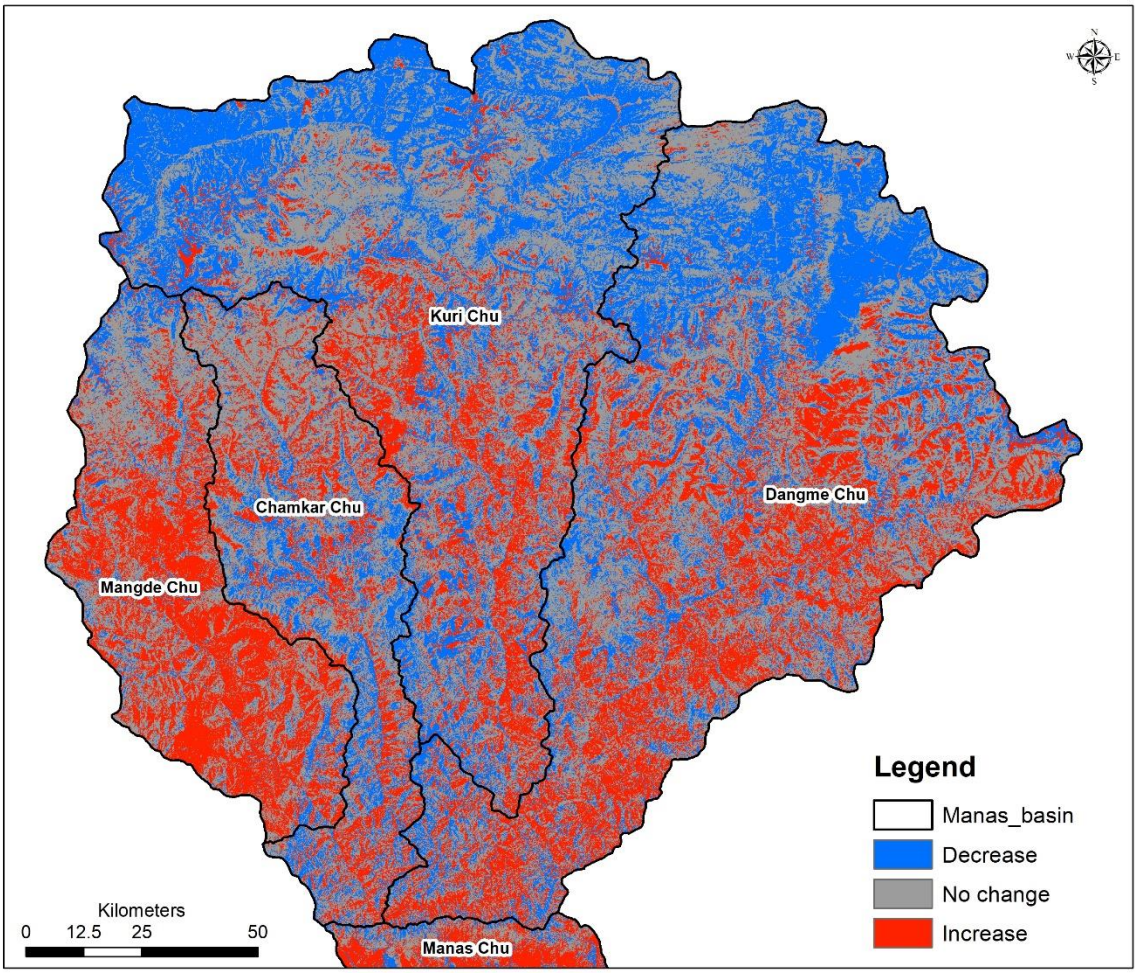

Figure 3.9 NDVI difference image (1990-2020) showing change and no change areas in upper catchments of Manas-Beki basin

Vegetation area maps were prepared for each year, 1990, 2000, 2010, and 2020 using the best threshold value for differentiating between vegetation and no vegetation areas, selected after careful observation of the satellite images and the NDVI values during the month of December. The final vegetation maps are shown in Figure 3.10. Areas under vegetation for each year and each sub-basin were analyzed and the percentage areas of each basin and the overall area are depicted in Figure 3.11. The analysis of vegetation areas shows that the areas have increased from 1990 to 2020. Vegetation area in the entire upper catchment including all four glaciated sub-basins increased from ~23.9% to ~35.7% (~11.8%) from 1990 to 2020. Maximum change is observed in the western basin of Mangde Chu (~21.9%) and minimum change is observed in Kuri Chu basin (~6.5%) and the results are consistent with results obtained from preliminary analysis of the NDVI difference image.

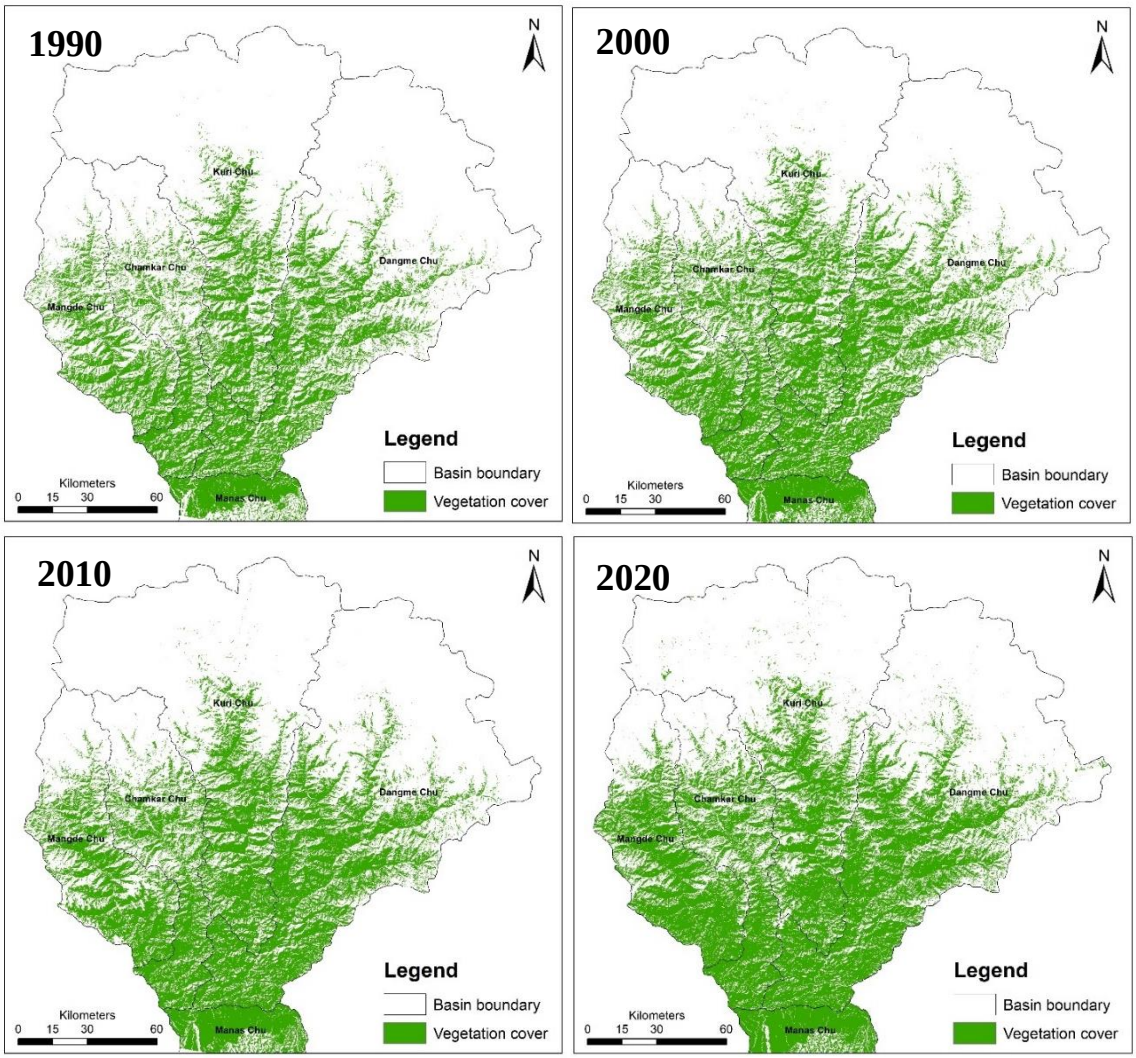

Figure 3.10 Vegetation cover area based on NDVI for Manas-Beki upper catchments (1990, 2000, 2010 and 2020)

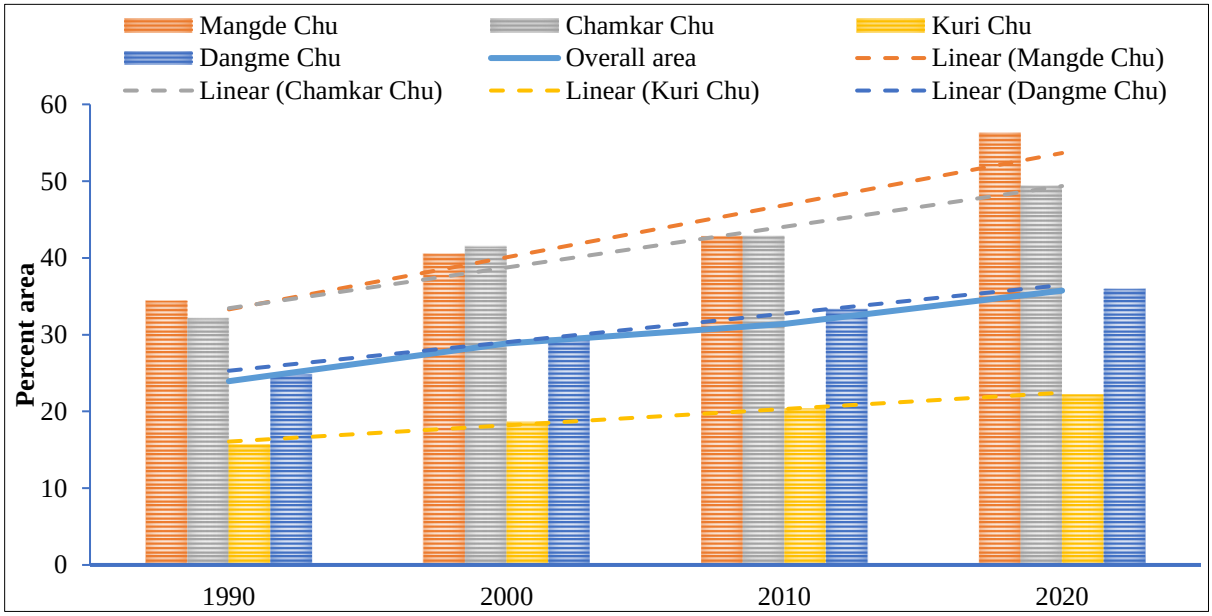

Figure 3.11 Vegetation area changes in percentage from 1990-2020 in Manas-Beki upper catchments

3.3.3 Snow cover changes in the upper catchments

Snow cover areas for the same season (December) for the entire catchment area were extracted from the Landsat-based NDVI, NDSI, and band ratio between NIR and MIR images of 1990, 2000, 2010, and 2020 (Figure 3.12). The percentage areas of snow coverage during the same season within the entire upper catchments and in individual sub-basins were analyzed and it is observed that the snow cover areas have decreased from ~10.9% to ~5.7% (~5.2%) from 1990 to 2020 (Figure 3.13). Decadal changes show that for the entire glaciated upper catchment area, the snow cover area decreased between 1990 to 2000 but increased thereafter. Analysis of snow-covered areas for individual sub-basins shows a decrease in all areas. Maximum change is observed in the eastern basin of Dangme Chu (~7.6%) and gradually decreases westward. The minimum change is observed in Mangde Chu basin (~2.6%).

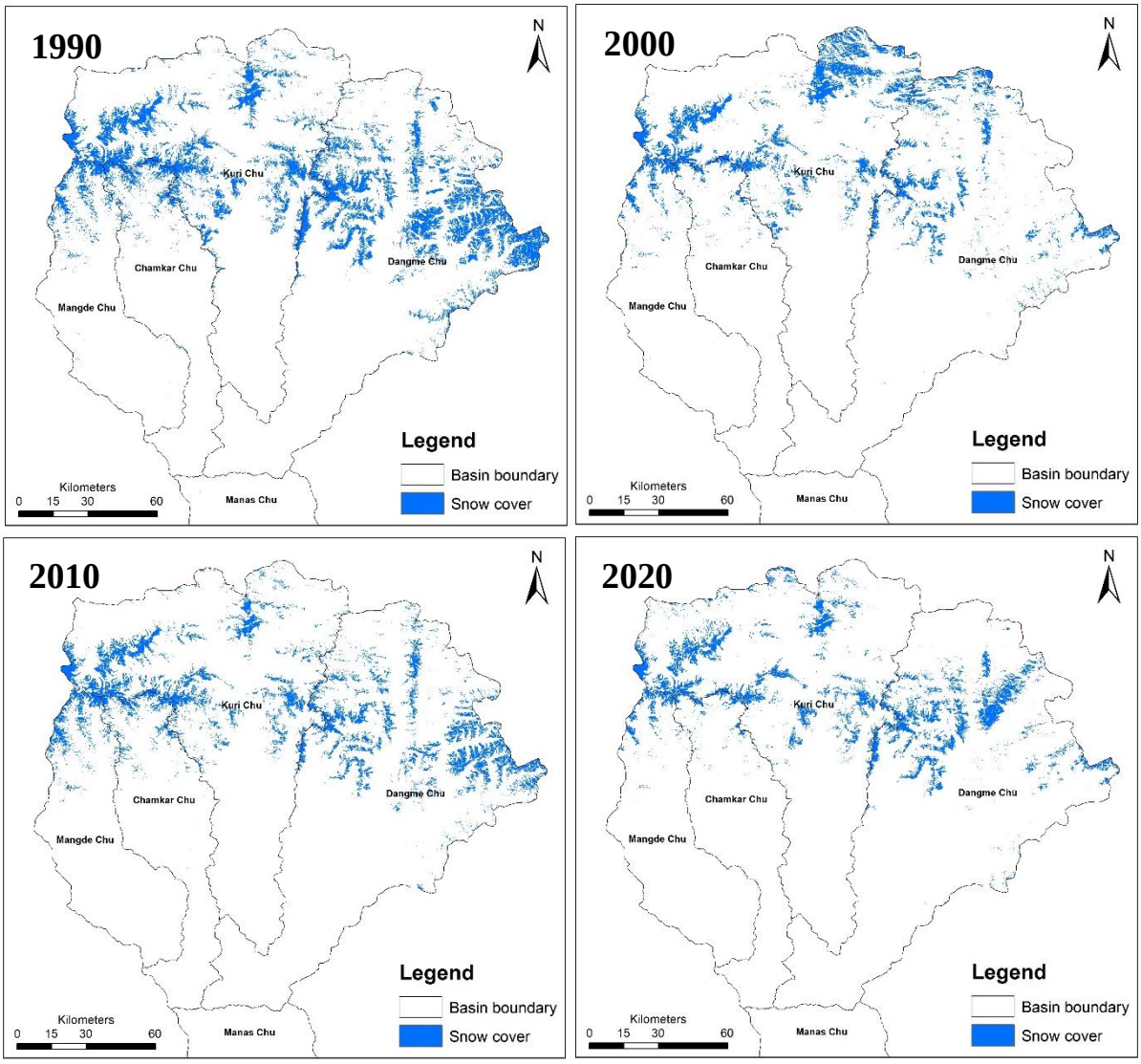

Figure 3.12 Snow cover area based on NDSI for Manas-Beki upper catchments (1990, 2000, 2010 and 2020)

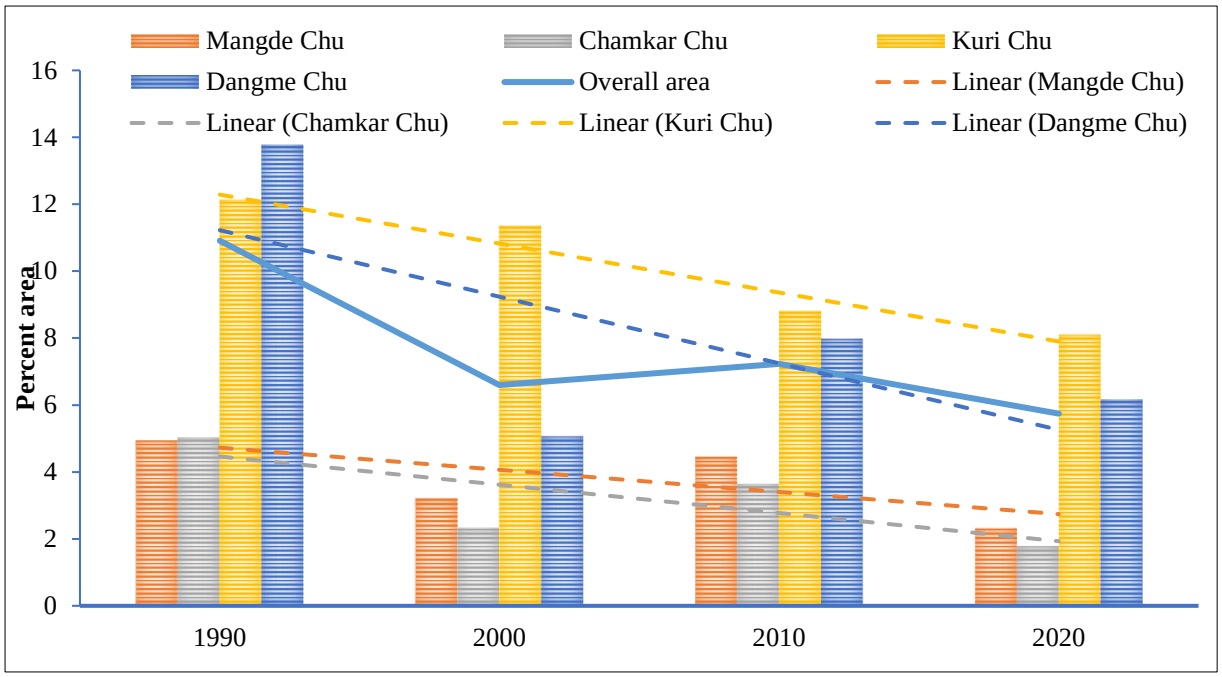

Figure 3.13 Snow cover area changes in percentage from 1990-2020 in Manas-Beki upper catchments

3.3.4 Seasonal snow cover changes

Since snow cover is a purely seasonal land cover class, so GEE was used to extract NDSI values for each season from 1990 to 2020 to understand the seasonal changes. Four seasons were considered for every 3 months of the year and Landsat daily NDSI composites for the entire study area were generated using maximum function to extract maximum snow cover during the identified seasons. The final snow cover maps showing the maximum snow-covered areas during the season were generated after extracting the areas with NDSI values greater than 0.4. The seasonal snow cover maps for the Manas-Beki basin for 1990 and 2020 are shown in Figure 3.14. Snow cover areas were extracted for every season from 1990 to 2020 and the maximum snow cover areas were analyzed.

The overall areas covered with snow from 1990 to 2020 is showing a decreasing trend in all the seasons. The maximum change is observed during the months of Jan-Mar, followed by the Oct-Dec season, though annual variations in snow-covered areas are very erratic throughout the observation period. Figure 3.15 shows the annual variations in maximum snow cover area in percentages for the Manas-Beki basin in different seasons. The values are highest for Jan-Mar and range from 20% to more than 40% in the basin. The minimum snow cover is observed in the months of July-Sep when the values mostly range between 3% to 10% of the total area.

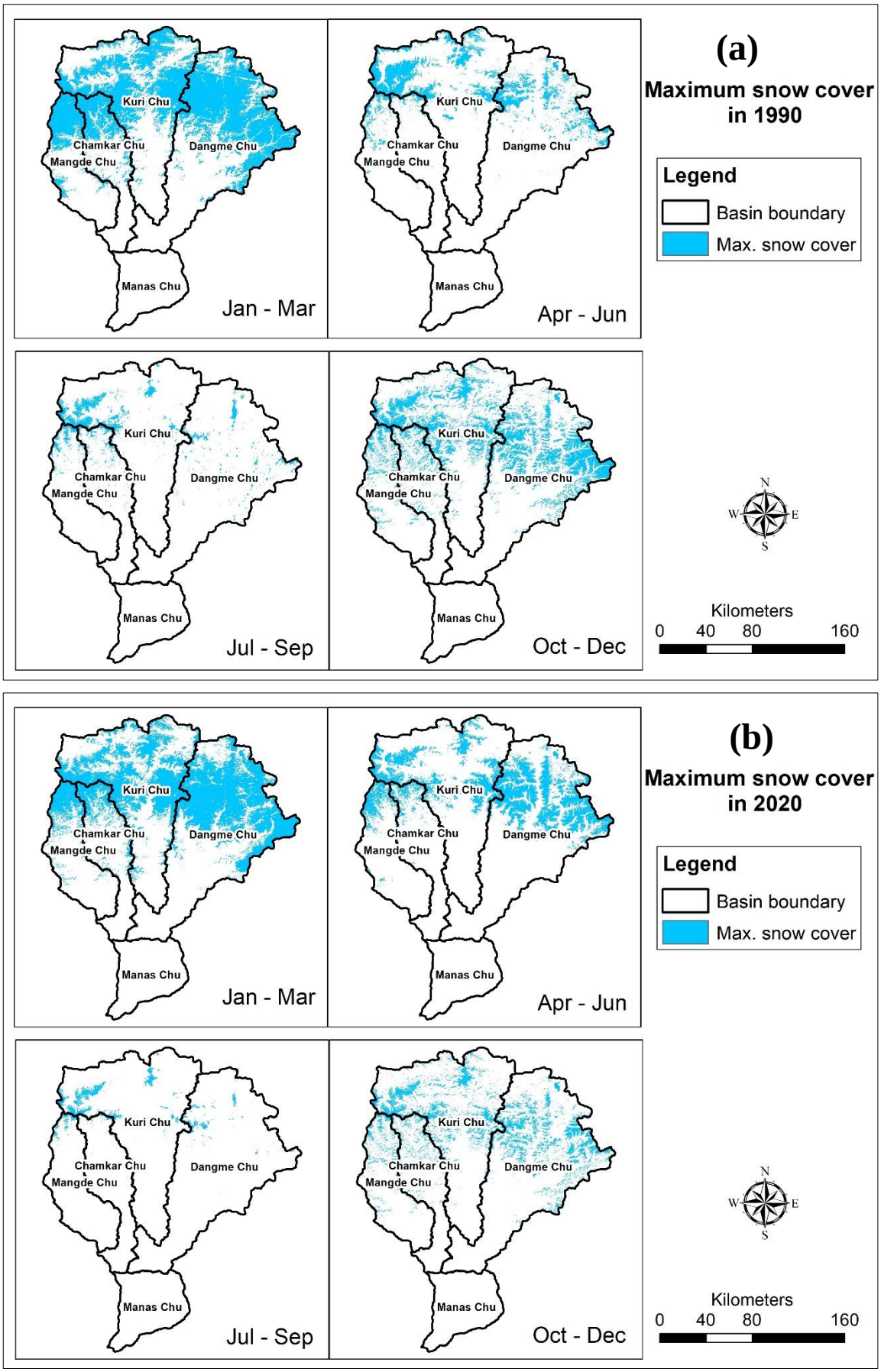

Figure 3.14 Seasonal snow cover area in (a)1990 and (b) 2020) for the Manas-Beki basin

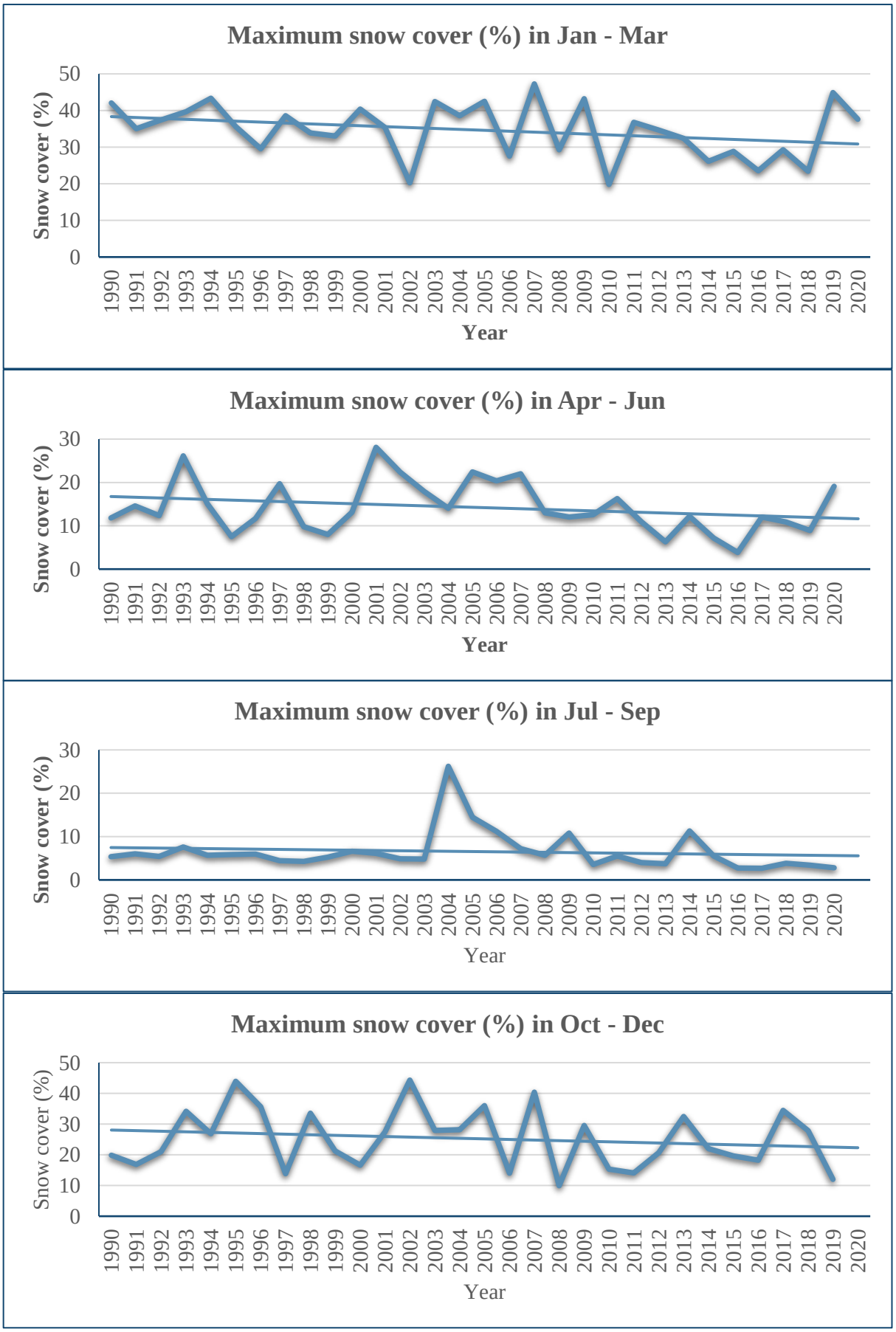

Figure 3.15 Seasonal snow cover area changes in percentage (1990 - 2020) for the Manas-Beki basin

GEE was also used to analyze the trends in snow cover area change during the period 1990 to 2020. Since snow cover maps using Landsat data were chosen for the month of December for analysis, the trend was analyzed during the same month over the years. The graphs for the four glaciated sub-basins of Manas-Beki basin are shown in Figure 3.16 (a-d) and in all the basins, there is a slight decrease in average snow cover area visualized as a percentage to the total area of the sub-basin. The highest decrease is observed in the easternmost basin of Dangme Chu. The results are in parallel with the results of the overall snow cover analysis carried out in the Manas-Beki basin using satellite data.

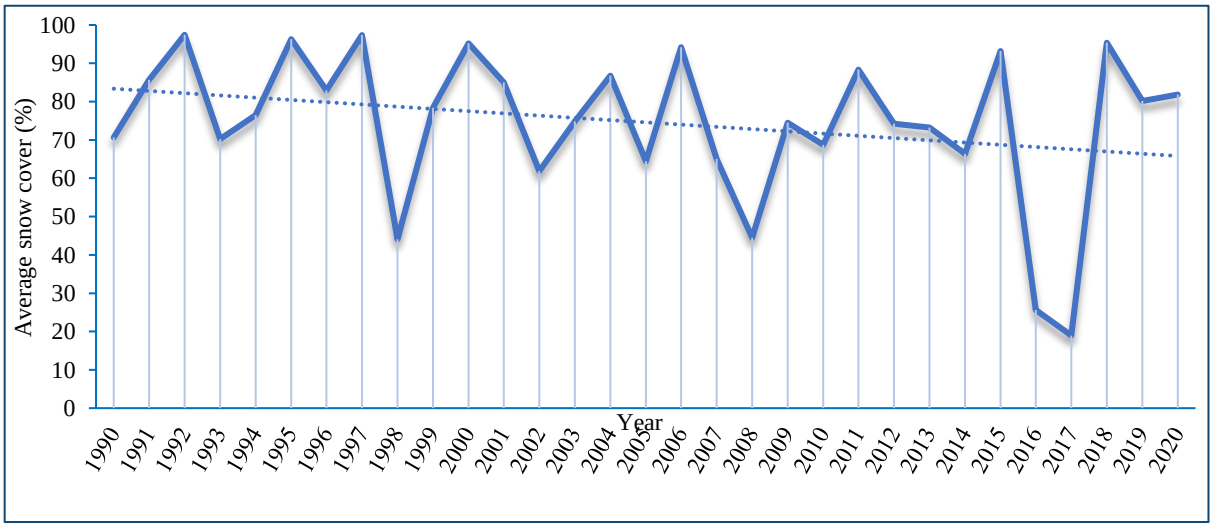

Figure 3.16(a) Average snow cover (in %) in Mangde Chu Basin for December (1990-2020)

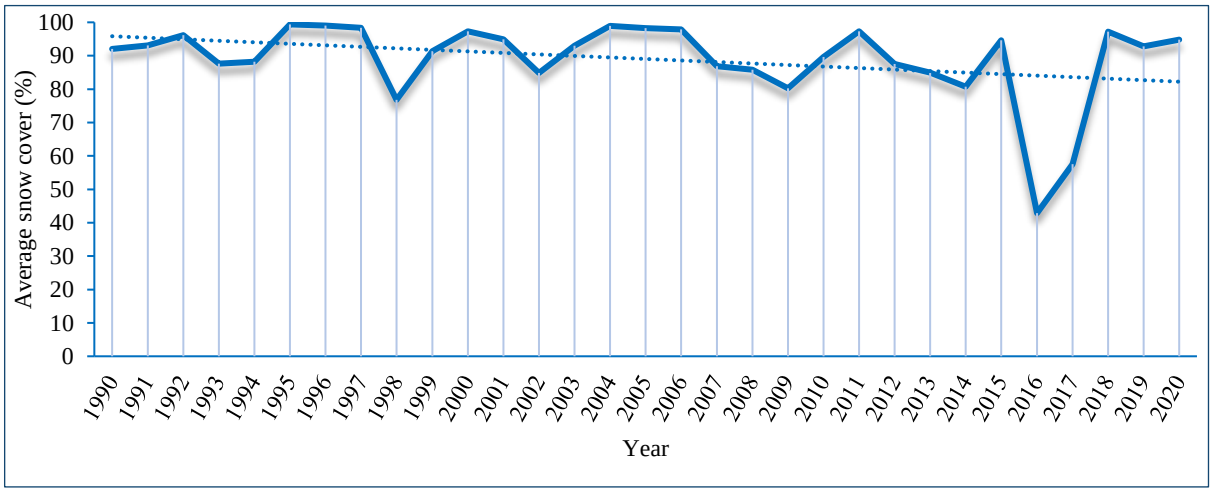

Figure 3.16(b) Average snow cover (in %) in Chamkar Chu Basin for December (1990-2020)

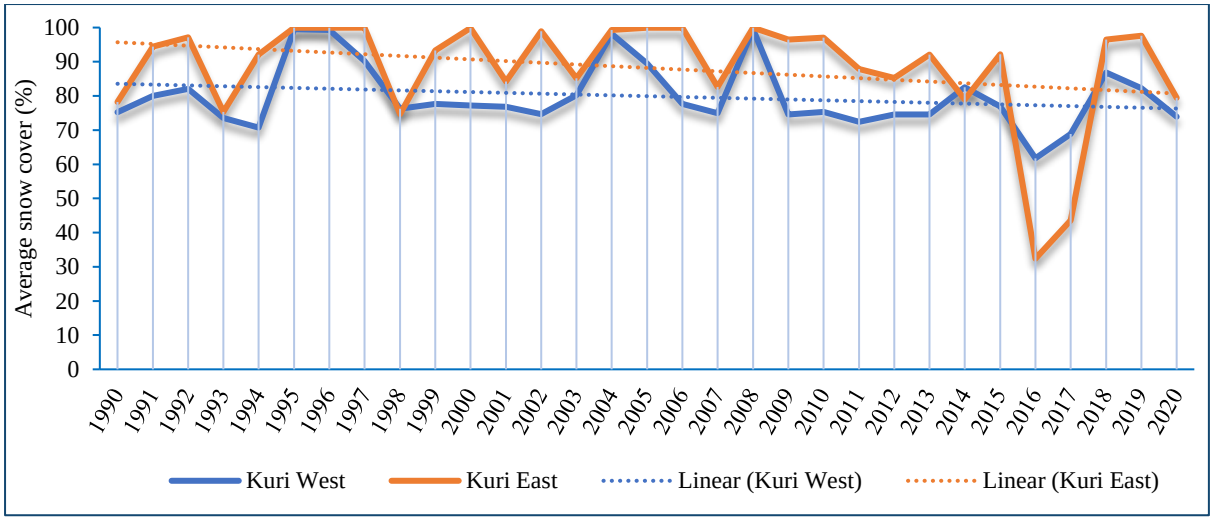

Figure 3.16(c) Average snow cover (in %) in Kuri Chu Basin for December (1990-2020)

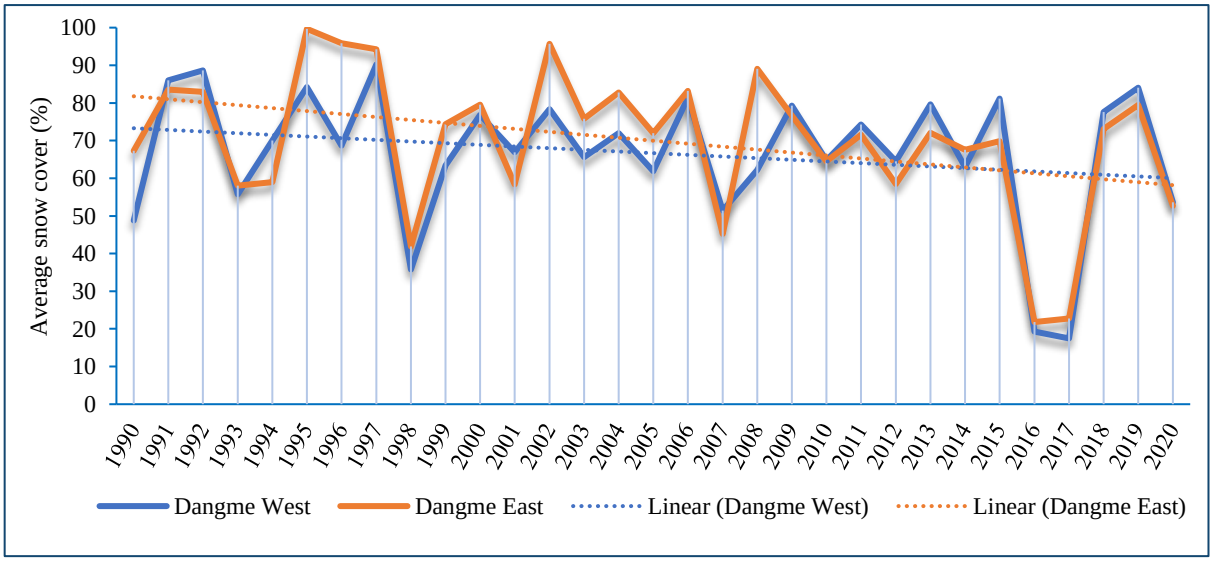

Figure 3.16(d) Average snow cover (in %) in Dangme Chu Basin for December (1990-2020)

3.3.5 Snow and vegetation changes with elevation

The change analysis for snow and vegetation cover in the upper glaciated sub-basins of Manas-Beki river basin carried out for every decade from 1990 to 2020 using Landsat satellite data was compared at different altitudes to observe the altitudinal variations in change. Figure 3.17 shows the variability of vegetation cover areas with elevation from 1990 to 2020. It is clearly seen that the maximum variability is between 2000-3000 m elevations even though vegetation cover is seen up to almost 6000-6500 m elevations. The values are also distinctly increased in the span of a decade and the maximum areas are observed in 2020.

Changes in snow cover from 1990 to 2020 show considerable change between 5000 m to 5500 m elevation levels (Figure 3.18). The total area of snow cover in the basin is also distinctly decreasing over the years with the maximum decrease in the 5000-5500 m elevation range.

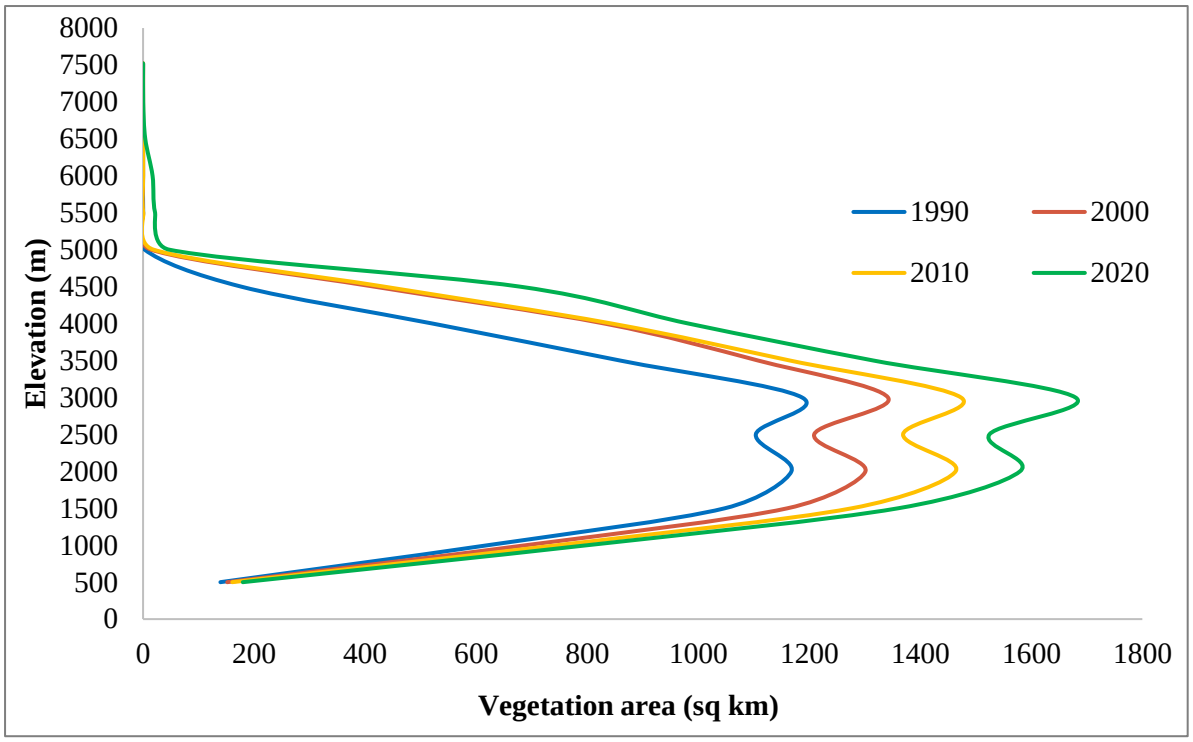

Figure 3.17 Vegetation area changes with elevation from 1990-2020 for the Manas-Beki basin

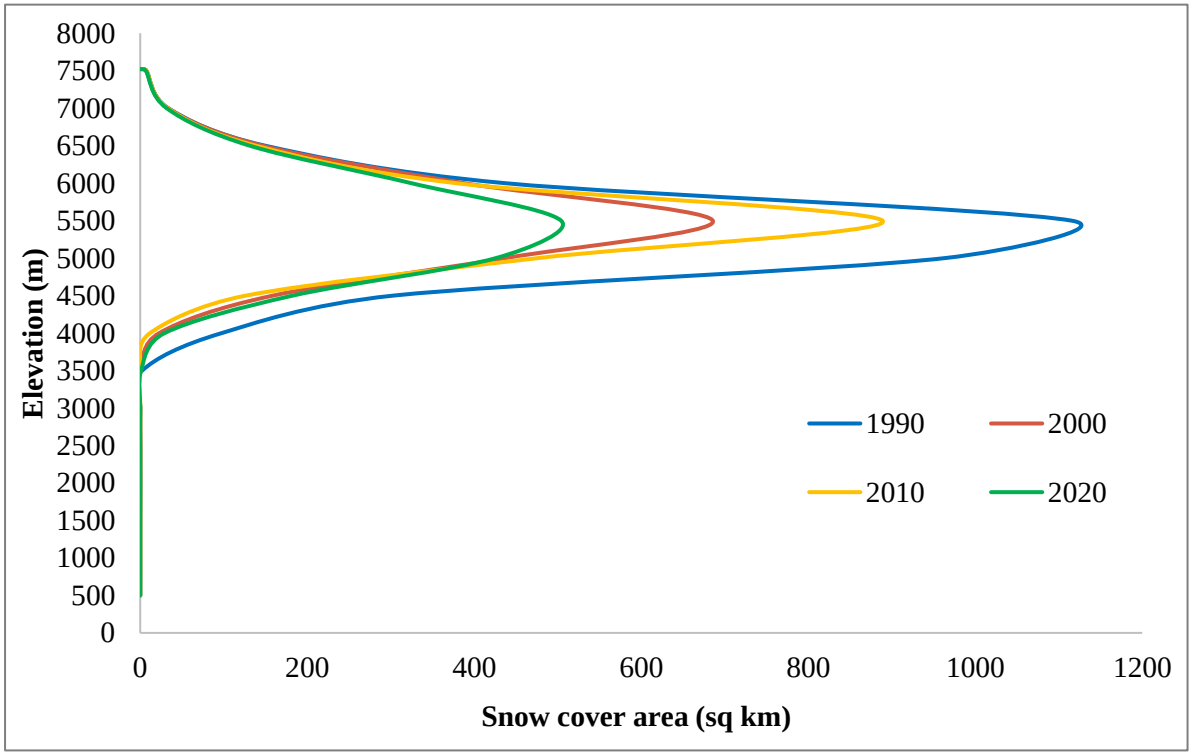

Figure 3.18 Snow cover area changes with elevation from 1990-2020 for the Manas-Beki basin

The overlap region between snow and vegetation cover area distribution at different elevation ranges in the Manas-Beki basin shows changes in snow line altitude. On observation of the overlap of the two graphs, it is seen that the point of interaction between the snow and vegetation areas has increased from 1990 to 2020 showing that the snow altitude have gone up over the years (Figure 3.19).

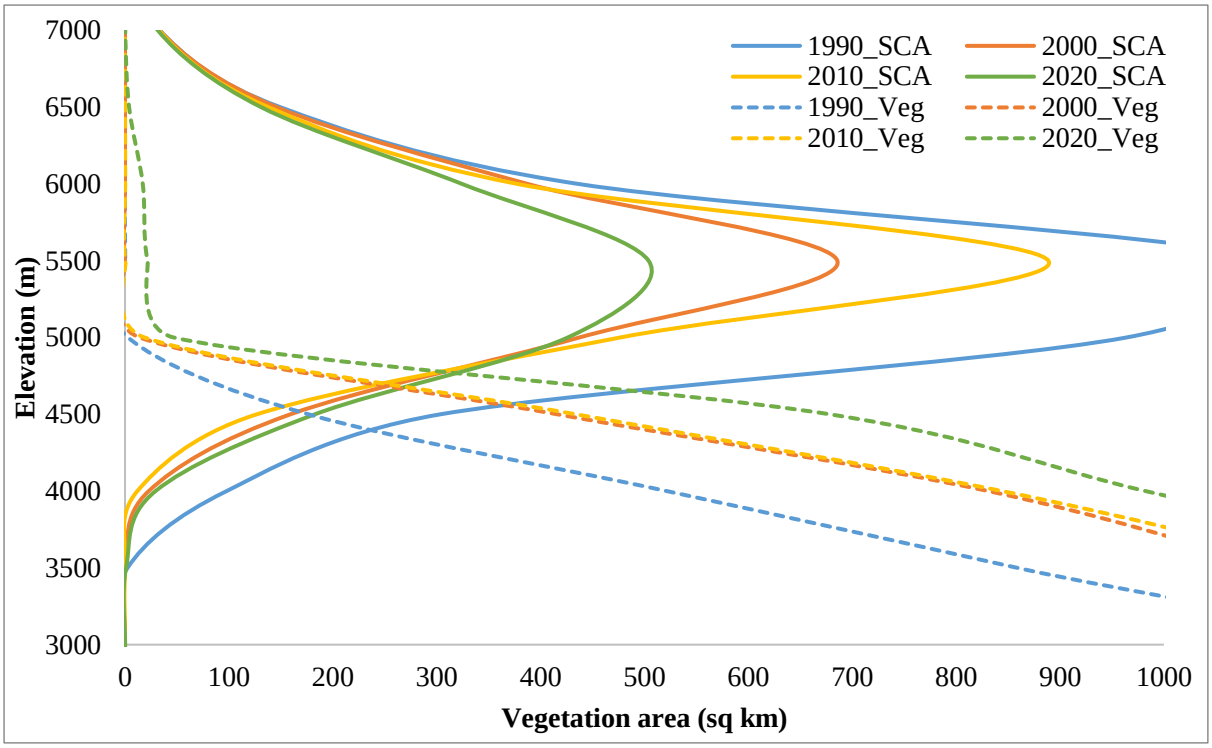

Figure 3.19 Snow and vegetation area changes with elevation for overlap region in upper Manas-Beki basin, 1990-2020

3.4 Discussion and summary

LULC changes in the floodplains adjacent to the Manas-Beki river show highly variable characteristics from 1990 to 2020. The most significant changes in the LULC classes are the increase in water areas (~28 km^2) between 2010-2020, loss of vegetation (~24.5 km^2), and loss of grassland areas (~33 km^2) during 1990-2000. Highly dynamic changes are noticed in the sand class during 1990-2000 (increase ~49 km^2) and 2010-2020 (decrease ~37 km^2).

Vegetation areas (comprising forest and tree-clad areas) and natural grasslands show a decrease in 2000 from 1990 but increase slightly in 2010 and 2020. Agricultural areas and sand-deposited areas show an increase from 1990 to 2000 but decrease slightly between 2010 and 2020. The only LULC category that has exponentially increased over the years is the settlement class which comprises the built-up areas. Settlement areas have nearly more than doubled every

decade with an almost 16 times overall increase in area from 1990 to 2020. The water class had shown a slightly decreasing trend from 1990 to 2010 but increased considerably from 2010 to 2020. Various factors might be attributed to the LULC dynamics in the region and channel shifts and changes in the river morphology (which were analyzed in the previous chapter), might be one of the major factors. Researchers have indicated that fluvial dynamics is one of the major drivers of LULC dynamics especially in highly populated alluvial floodplain regions which are periodically exposed to flooding [26, 30, 59]. In the present study, it is observed that the river has frequently changed course during the three decades of analysis and erosion was the dominant process, especially in the areas above the highway crossing which were mainly forest and grassland areas during 1990-2000. This can be related to the decrease in these LULC classes during the period. Sand areas have increased due to the conversion of the active channel course into deposition areas. Deposition is also a dominant process, particularly between 2000 and 2020.

Human alterations to the floodplains particularly for use as agricultural lands or built-up areas result in changes in land cover categories, and is another driver of LULC changes [60]. In the present study, it is observed that the settlement areas within the study area have increased exponentially indicating the increased impact of human population in the area. Every decade, more than 100 km^2 of land from other categories of LULC have been converted to agricultural land, although agricultural areas have also extensively been converted into other LULC categories over the years.

Chronic flooding in the lower parts of the floodplain is also being attributed by researchers to the changes in LULC, particularly related to water and sand deposition areas [26, 61, 62]. Dynamics in flooding incidences have also been reported to be linked to observed changes in climate change and associated phenomena such as increased precipitation and snow melt in the upper reaches of the basin [63, 64]. In the case of Manas-Beki floodplains, it is observed that the water class has increased considerably between 1990 and 2020, and field observations confirmed that the chronically flooded lower floodplain of the Manas-Beki river has been utilized for fisheries in recent years. High deposition of sand is also associated with the frequent incidences of flash floods in the study area.

Changes in vegetation and snow cover in the upper glaciated sub-basins of Manas-Beki river represent an increase in vegetation and a decrease in snow cover. This correlates with other findings for the Himalayan region and is linked to natural factors, primarily climate change

since human impacts on land cover at higher elevations are minimal [57, 65-70]. Analysis of NDVI values shows an increase in NDVI values in the last decade (2010-2020) in all the four sub-basins (Mangde, Chamkar, Kuri, and Dangme), whereas the change is negligible during the previous decades. It is also observed that the change is more in the west than the east, which is in consistence with the observations of Mishra and Mainali [65]. Almost all studies on the Himalayan landscape, including limited studies in the Bhutan region, report a decline in the snow cover area in recent years [68-70]. The ERA5 reanalysis dataset was used in this study to correlate the results. The findings show that the snow cover area has decreased from 1990 to 2020. Analysis of seasonal snow cover shows a considerable decline in maximum snow cover area during the months of Jan-Mar followed by Oct-Dec. Seasonal and directional variations as observed in the present study were also reported by other researchers for the Himalayan region [71, 72].

Based on elevation, snow and vegetation changes observed at different elevations suggest the highest variations in vegetation between the 2000 to 3000 m altitudes and the highest variation in snow cover between 5000 to 5500 m altitudes. Vegetation cover is also observed to increase at higher elevations while snow cover is decreasing indicating a shift in the tree line and snow line altitudes. Similar trends have been reported from other parts of the Himalayas by researchers [57, 58, 65, 69] and the changes have been attributed to be an indicator of climate change influence on the area. These observed changes in vegetation and snow cover in the upper catchments are likely to affect the streamflow in the basin impacting downstream water availability [15, 73, 74].

3.5 References

[1] Pielke Sr., R.A. Land Use and Climate Change. *Science*, 310:1625-1626, 2005. DOI: https://doi.org/10.1126/science.1120529.

[2] Roy, P.S., Ramachandran, R.M., Paul, O., Thakur, P.K., Ravan, S., Behera, M.D., Sarangi, C., and Kanawade, V.P. Anthropogenic Land Use and Land Cover Changes—A Review on Its Environmental Consequences and Climate Change. *Journal of the Indian Society of Remote Sensing*, 50, 1615–1640, 2022. DOI: https://doi.org/10.1007/s12524-022-01569-w.

[3] Dale, V.H. The relationship between land-use change and climate change. *Ecological Applications*, 7(3):753-769, 1997. DOI: https://doi.org/10.1890/1051-0761(1997)007[0753:TRBLUC]2.0.CO;2.

[4] Basumatary, H., Devi, H.S., Borah, S.B., and Das, A.K. Land cover dynamics and their driving factors in a protected floodplain ecosystem. *River Research and Applications*, 37(1):627–643, 2021. DOI: https://doi.org/10.1002/rra.3775.

[5] Gurnell, A. M., and Gregory, K. J. Interactions between semi-natural vegetation and hydrogeomorphological processes. *Geomorphology*, 13(1-4):49–69, 1995. DOI: https://doi.org/10.1016/0169-555x(95)00030-9.

[6] Fitzpatrick, F. A., and Knox, J. C. Spatial and temporal sensitivity of hydrogeomorphic response and recovery to deforestation, agriculture, and floods. *Physical Geography*, 21(2):89–108, 2000. DOI: https://doi.org/10.1080/02723646.2000.10642701.

[7] Asselman, N.E.M., Middelkoop, H., and van Dijk, P.M. The impact of changes in climate and land use on soil erosion, transport and deposition of suspended sediment in the River Rhine. Hydrological Processes, 17(16):3225-3244, 2003. DOI: https://doi.org/10.1002/hyp.1384.

[8] Poff, N.L., Bledsoe, B.P., and Cuhaciyan, C.O. Hydrologic variation with land use across the contiguous United States: Geomorphic and ecological consequences for stream ecosystems. *Geomorphology*, 79(3–4):264-285, 2006. DOI: https://doi.org/10.1016/j.geomorph.2006.06.032.

[9] Pervez, M.S., and Henebry, G.M. Assessing the impacts of climate and land use and land cover change on the freshwater availability in the Brahmaputra River basin. *Journal of Hydrology: Regional Studies*, 3:285-311, 2015. DOI: https://doi.org/10.1016/j.ejrh.2014.09.003.

[10] Deng, X., Shi, Q., Zhang, Q., Shi, C., and Yin, F. Impacts of land use and land cover changes on surface energy and water balance in the Heihe River Basin of China, 2000–2010. *Physics and Chemistry of the Earth, Parts A/B/C*, 79–82: 2-10, 2015. DOI: https://doi.org/10.1016/j.pce.2015.01.002.

[11] Saddique, N., Mahmood, T., and Bernhofer, C. Quantifying the impacts of land use/land cover change on the water balance in the afforested River Basin, Pakistan. *Environmental Earth Sciences*, 79:448, 2020. DOI: https://doi.org/10.1007/s12665-020-09206-w.

[12] Tadese, M., Kumar, L., Koech, R., and Kogo, B.K. Mapping of land-use/land-cover changes and its dynamics in Awash River Basin using remote sensing and GIS. Remote Sensing Applications: Society and Environment, 19:100352, 2020. DOI: https://doi.org/10.1016/j.rsase.2020.100352.

[13] Meyer, W. B., and Turner, B. L. Human Population Growth and Global Land-Use/Cover Change. *Annual Review of Ecology and Systematics*, 23(1):39–61, 1992. DOI: https://doi.org/10.1146/annurev.es.23.110192.

[14] Lambin, E. F., Turner, B. L., Geist, H. J., Agbola, S. B., Angelsen, A., Bruce, J. W., … Xu, J. The causes of land-use and land-cover change: moving beyond the myths. *Global Environmental Change*, 11(4):261–269, 2001. DOI: https://doi.org/10.1016/s0959-3780(01)00007-3.

[15] Lambin, E.F., Geist, H.J., and Lepers, E. Dynamics of Land-Use and Land-Cover Change in Tropical Regions. *Annual Review of Environment and Resources*, 28(1):205-241, 2003. DOI: https://doi.org/10.1146/annurev.energy.28.050302.105459.

[16] Geist, H., McConnell, W., Lambin, E.F., Moran, E., Alves, D., and Rudel, T. Causes and Trajectories of Land-Use/Cover Change. In Lambin, E.F., Geist, H., editors, *Land-Use and Land-Cover Change*, Global Change - The IGBP Series, pages 41-70, ISBN: 978-3-540-32201-6, Springer, Berlin, Heidelberg, 2006. DOI: https://doi.org/10.1007/3-540-32202-7_3.

[17] Davies-Barnard, T., Valdes, P. J., Singarayer, J. S., Wiltshire, A. J., and Jones, C. D. Quantifying the relative importance of land cover change from climate and land use in the representative concentration pathways. *Global Biogeochemical Cycles*, 29:842– 853, 2015. DOI: https://doi.org/110.1002/2014GB004949.

[18] Turner, B.L., Lambin, E.F., and Verburg, P.H. From land-use/land-cover to land system science. *Ambio*, 50:1291–1294, 2021. DOI: https://doi.org/10.1007/s13280-021-01510-4.

[19] Arias, M.E., Cochrane, T.A., Piman, T., Kummu, M., Caruso, B.S., and Killeen, T.J. Quantifying changes in flooding and habitats in the Tonle Sap Lake (Cambodia) caused by water infrastructure development and climate change in the Mekong Basin. *Journal of Environmental Management*, 112: 53-66, 2012. DOI: https://doi.org/10.1016/j.jenvman.2012.07.003.

[20] Maddheshiya, S.K., Jha, M., Tignath, S., Singh, N. Hydrogeomorphic and Spatio-Temporal Analysis of Riverine Wetlands in the Interfluvial Zone of Ganga and Sai Rivers, Uttar Pradesh, India. *Wetlands*, 43:9, 2023. DOI: https://doi.org/10.1007/s13157-022-01654-3.

[21] Frankl, A., Nyssen, J., De Dapper, M., Haile, M., Billi, P., Munro, R.N., Deckers, J., and Poesen, J. Linking long-term gully and river channel dynamics to environmental change using repeat photography (Northern Ethiopia). *Geomorphology*, 129(3–4): 238-251, 2011. DOI: https://doi.org/10.1016/j.geomorph.2011.02.018.

[22] Gurnell, A.M., Corenblit, D., de Jalón, D.G., del Tánago, M.G., Grabowski, R. C., O'Hare, M.T., and Szewczyk, M. A Conceptual Model of Vegetation–hydrogeomorphology Interactions Within River Corridors. *River Research and Applications*, 32(2): 142-163, 2016. DOI: https://doi.org/10.1002/rra.2928.

[23] Fernandes, M.R., Aguiar, F.C., Martins, M.J., Rivaes, R., and Ferreira, M.T. Long-term human-generated alterations of Tagus River: Effects of hydrological regulation and land-use changes in distinct river zones. *Catena*, 188: 104466, 2020. DOI: https://doi.org/10.1016/j.catena.2020.104466.

[24] Han, M., and Brierley, G. Assessment of the geo-eco-hydrological condition of anabranching reaches in the Source Zone of the Yellow River, western China. *River Research and Applications*, 37(5):683-698, 2021. DOI: https://doi.org/10.1002/rra.3786.

[25] Okeke, C.A.U., Uno, J., Academe, S., Emenike, P.C., Abam, T.K.S., and Omole, D.O. An integrated assessment of land use impact, riparian vegetation and lithologic variation on streambank stability in a peri-urban watershed (Nigeria). *Scientific Reports*, 12:10989, 2022. DOI: https://doi.org/10.1038/s41598-022-15008-w.

[26] Hazarika, N., Das, A.K., Borah, S.B. Assessing land-use changes driven by river dynamics in chronically flood affected Upper Brahmaputra plains, India, using RS-GIS techniques. *The Egyptian Journal of Remote Sensing and Space Sciences*, 18(1):107–118, 2015. DOI: http://dx.doi.org/10.1016/j.ejrs.2015.02.001.

[27] Fan, F., Wang, Y., and Wang, Z. Temporal and spatial change detecting (1998–2003) and predicting of land use and land cover in Core corridor of Pearl River Delta (China) by using TM and ETM+ images. Environmental Monitoring and Assessment, 137:127–147, 2008. DOI: https://doi.org/10.1007/s10661-007-9734-y.

[28] Kline, M., and Cahoon, B. Protecting River Corridors in Vermont. Journal of the American Water Resources Association, 46(2): 227-236, 2010. DOI: https://doi.org/10.1111/j.1752-1688.2010.00417.x.

[29] Eniolorunda, N.B., Mashi, S.A., and Nsofor, G.N. Toward achieving a sustainable management: characterization of land use/land cover in Sokoto Rima floodplain, Nigeria. Environment, *Development and Sustainability*, 19:1855–1878, 2017. DOI: https://doi.org/10.1007/s10668-016-9831-6.

[30] Saikia, L., Mahanta, C., Mukherjee, A., and Borah, S.B. Erosion–deposition and land use/land cover of the Brahmaputra river in Assam, India. *Journal of Earth System Science*, 128:211, 2019. DOI: https://doi.org/10.1007/s12040-019-1233-3.

[31] Köplin, N., Schädler, B., Viviroli, D., and Weingartner, R. The importance of glacier and forest change in hydrological climate-impact studies. *Hydrology and Earth System Sciences*, 17(2):619–635, 2013. DOI: https://doi.org/10.5194/hess-17-619-2013.

[32] Geng, X., Wang, X., Yan, H., Zhang, Q., and Jin, G. Land Use/Land Cover Change Induced Impacts on Water Supply Service in the Upper Reach of Heihe River Basin. *Sustainability*, 7(1):366-383, 2015. DOI: https://doi.org/10.3390/su7010366.

[33] Severin, H., Ulrike, A., Monika, B., Thomas, B., Christian, H., Martin, K., Leena, R., Yvonne, S., and Gertrud, H. Land Use and Cover Change in the Industrial Era: A Spatial Analysis of Alpine River Catchments and Fluvial Corridors. *Frontiers in Environmental Science*, 9:647247, 2021. DOI: https://doi.org/10.3389/fenvs.2021.647247.

[34] Allan, D., Erickson, D., and Fay, J. The influence of catchment land use on stream integrity across multiple spatial scales. *Freshwater Biology*, 37(1):149-161, 1997. DOI: https://doi.org/10.1046/j.1365-2427.1997.d01-546.x.

[35] Devito, K.J., Hokanson, K.J., Moore, P.A., Kettridge, N., Anderson, A.E., Chasmer, L., Hopkinson, C., Lukenbach, M.C., and Mendoza, C.A. Landscape controls on long-term runoff in subhumid heterogeneous Boreal Plains catchments. *Hydrological Processes*, 31(15):2737-2751, 2017. DOI: https://doi.org/10.1002/hyp.11213.

[36] Bavay, M., Lehning, M., Jonas, T., and Löwe, H. Simulations of future snow cover and discharge in Alpine headwater catchments. *Hydrological Processes*, 23(1):95-108, 2009. DOI: https://doi.org/10.1002/hyp.7195.

[37] Bavay, M., Grünewald, T., and Lehning, M. Response of snow cover and runoff to climate change in high Alpine catchments of Eastern Switzerland. *Advances in Water Resources*, 55: 4-16, 2013. DOI: https://doi.org/10.1016/j.advwatres.2012.12.009.

[38] Hohensinner, S., Atzler, U., Fischer, A., Schwaizer, G., and Helfricht, K. Tracing the Long-Term Evolution of Land Cover in an Alpine Valley 1820–2015 in the Light of Climate, Glacier and Land Use Changes. *Frontiers in Environmental Science*, 9:683397, 2021. DOI: https://doi.org/10.3389/fenvs.2021.683397.

[39] Nepal, S., Krause, P., Flügel, W.-A., Fink, M., and Fischer, C. Understanding the hydrological system dynamics of a glaciated alpine catchment in the Himalayan region using the J2000 hydrological model. *Hydrological Processes*, 28(3):1329-1344, 2014. DOI: https://doi.org/10.1002/hyp.9627.

[40] Schickhoff, U., Singh, R.B., and Mal, S. Climate Change and Dynamics of Glaciers and Vegetation in the Himalaya: An Overview. In Singh, R., Schickhoff, U., Mal, S., editors, *Climate Change, Glacier Response, and Vegetation Dynamics in the Himalaya*, pages 1-26, ISBN: 978-3-319-28975-5, Springer, Cham, 2016. DOI: https://doi.org/10.1007/978-3-319-28977-9_1.

[41] Anderson, K., Fawcett, D., Cugulliere, A., Benford, S., Jones, D., and Leng, R. Vegetation expansion in the subnival Hindu Kush Himalaya. *Global Change Biology*, 26(3):1608-1625, 2020. DOI: https://doi.org/10.1111/gcb.14919.

[42] Haq, M.A., Baral, P., Yaragal, S., and Pradhan, B. Bulk Processing of Multi-Temporal Modis Data, Statistical Analyses and Machine Learning Algorithms to Understand Climate Variables in the Indian Himalayan Region. *Sensors*, 21:7416, 2021. DOI: https://doi.org/10.3390/s21217416.

[43] Gilani, H., Shrestha, H.L., Murthy, M.S.R., Phuntso, P., Pradhan, S., Bajracharya, B., and Shrestha, B. Decadal land cover change dynamics in Bhutan. *Journal of Environmental Management*, 148: 91-100, 2015. DOI: https://doi.org/10.1016/j.jenvman.2014.02.014.

[44] Chhogyel, N., Kumar, L., and Bajgai, Y. Spatio-temporal landscape changes and the impacts of climate change in mountainous Bhutan: A case of Punatsang Chhu Basin. *Remote Sensing Applications: Society and Environment*, 18:100307, 2020. DOI: https://doi.org/10.1016/j.rsase.2020.100307.

[45] Paolini, L., Grings, F., Sobrino, J. A., Muñoz, J.C.J., Karszenbaum, H. Radiometric correction effects in Landsat multi-date/multi-sensor change detection studies. *International Journal of Remote Sensing*, 27(4):685-704, 2006. DOI: https://doi.org/10.1080/01431160500183057.

[46] Callahan, K.E. Validation of a radiometric normalization procedure for satellite derived imagery within a change detection framework. Master's thesis, Utah State University, Logan, Utah, 2003.

[47] Dai, X., and Khorram, S. The effects of image misregistration on the accuracy of remotely sensed change detection. *IEEE Transactions on Geoscience and Remote Sensing*, 36(5):1566-1577, 1998. DOI: https://doi.org/10.1109/36.718860.

[48] Jensen, J.R. *Introductory Digital Image Processing: A Remote Sensing Perspective*. Prentice Hall, Inc., Upper Saddle River, 2nd edition, New Jersey, USA, 1996.

[49] Irvin, B.J., Ventura, S.J., and Slater, B.K. Fuzzy and isodata classification of landform elements from digital terrain data in Pleasant Valley, Wisconsin. *Geoderma*, 77(2–4):137-154, 1997. DOI: https://doi.org/10.1016/S0016-7061(97)00019-0.

[50] Foody, G.M. Status of land cover classification accuracy assessment. *Remote Sensing of Environment*, 80(1):185–201, 2002. DOI: https://doi.org/10.1016/S0034-4257(01)00295-4.

[51] Congalton, R.G. A Review of Assessing the Accuracy of classifications of Remotely Sensed Data. *Remote Sensing of the Environment*, 37(1):35-46, 1991. DOI: https://doi.org/10.1016/0034-4257(91)90048-B.

[52] Munthali, M., Botai, J., Davis, N., and Abiodun, A. Multi-temporal Analysis of Land Use and Land Cover Change Detection for Dedza District of Malawi using Geospatial Techniques. *International Journal of Applied Engineering Research*, 14(5):1151-1162, 2019.

[53] Pettorelli, N., Vik, J.O., Mysterud, A., Gaillard, J-M., Tucker, C.J., and Stenseth, N.C. Using the satellite-derived NDVI to assess ecological responses to environmental change. *Trends in Ecology and Evolution*, 20(9): 503-510, 2005. DOI: https://doi.org/10.1016/j.tree.2005.05.011.

[54] Gandhi, G. M., Parthiban, S., Thummalu, N., and Christy, A. Ndvi: Vegetation Change Detection Using Remote Sensing and Gis – A Case Study of Vellore District. *Procedia Computer Science*, 57: 1199-1210, 2015. DOI: https://doi.org/10.1016/j.procs.2015.07.415.

[55] Huang, S., Tang, L., Hupy, J.P., Wang, Y., and Shao, G. A commentary review on the use of normalized difference vegetation index (NDVI) in the era of popular remote sensing. *Journal of Forestry Research*, 32:1–6, 2021. DOI: https://doi.org/10.1007/s11676-020-01155-1.

[56] Hayes, D., and Sader, S. Comparison of change-detection techniques for monitoring tropical forest clearing and vegetation regrowth in a time series. *Photogrammetric Engineering and Remote Sensing*, 67:1067-1075, 2001.

[57] Kumar, M., and Kumar, P. Snow Cover Dynamics and Timberline Change Detection of Yamunotri Watershed Using Multi-temporal Satellite Imagery. In Singh, R.B., Schickhoff, U., Mal, S., editors, *Climate Change, Glacier Response, and Vegetation Dynamics in the Himalaya*, pages 391–399, ISBN: 978-3-319-28975-5, Springer International Publishing, 2016. DOI: https://doi.org/10.1007/978-3-319-28977-9_20.

[58] Racoviteanu, A. E., Rittger, K., and Armstrong, R. An Automated Approach for Estimating Snowline Altitudes in the Karakoram and Eastern Himalaya From Remote Sensing. *Frontiers in Earth Science*, 7:220, 2019. DOI: https://doi.org/10.3389/feart.2019.00220.

[59] Beale, J., Grabowski, R.C., Lokidor, P.L., Vercruysse, K., and Simms, D.M. Vegetation cover dynamics along two Himalayan rivers: Drivers and implications of change. *Science of*

the Total Environment, 849:157826, 2022. DOI: http://dx.doi.org/10.1016/j.scitotenv.2022.157826.

[60] Alam, N., Saha, S., Gupta, S., and Chakraborty, S. Prediction modelling of riverine landscape dynamics in the context of sustainable management of floodplain: a Geospatial approach, *Annals of GIS*, 27(3):299-314, 2021. DOI: https://doi.org/10.1080/19475683.2020.1870558.

[61] Dhar, O.N., and Nandargi, S. A study of floods in the Brahmaputra basin in India. *International Journal of Climatology*, 20(7):771-781, 2000. DOI: https://doi.org/10.1002/1097-0088(20000615)20:7<771::AID-JOC518>3.0.CO;2-Z.

[62] Sah, R.K. and Das, A.K. Morphological Dynamics of the Rivers of Brahmaputra. *Journal of the Geological Society of India*, 92:441-448, 2018. DOI: https://doi.org/10.1007/s12594-018-1039-y.

[63] Bora, J. Climate Change and Its Effect on Hydrology and Threat to Biodiversity: A Study on Manas River (Upper Part) and the Manas National Park, Assam, India. In Sarma, A., Singh, V., Bhattacharjya, R., and Kartha, S., editors, *Urban Ecology, Water Quality and Climate Change*, volume 84 of *Water Science and Technology Library*, pages 157–168, ISBN: 978-3-319-74493-3, Springer, Cham, 2018. DOI: https://doi.org/10.1007/978-3-319-74494-0_12.

[64] Kumar. A., Mondal, S., and Lal, P. Analysing frequent extreme flood incidences in Brahmaputra basin, South Asia. *PLOS ONE* 17(8):e0273384, 2022. DOI: https://doi.org/10.1371/journal.pone.0273384.

[65] Mishra, N. B., and Mainali, K. P. Greening and browning of the Himalaya: Spatial patterns and the role of climatic change and human drivers. *Science of The Total Environment*, 587-588:326–339, 2017. DOI: https://doi.org/10.1016/j.scitotenv.2017.02.156.

[66] Bajracharya, B., Uddin, K., Chettri, N., Shrestha, B., and Siddiqui, S.A. Understanding Land Cover Change Using a Harmonized Classification System in the Himalaya. *Mountain Research and Development*, 30(2):143-156, 2010. DOI: https://doi.org/10.1659/MRD-JOURNAL-D-09-00044.1.

[67] Mishra, N.B., and Chaudhuri, G. Spatio-temporal analysis of trends in seasonal vegetation productivity across Uttarakhand, Indian Himalayas, 2000–2014. *Applied Geography*, 56:29-41, 2015. DOI: https://doi.org/10.1016/j.apgeog.2014.10.007.

[68] Gurung, D. R., Kulkarni, A. V., Giriraj, A., Aung, K. S., Shrestha, B., and Srinivasan, J. Changes in seasonal snow cover in Hindu Kush-Himalayan region. *The Cryosphere Discussions*, 5:755–777, 2011. DOI: https://doi.org/10.5194/tcd-5-755-2011.

[69] Maskey, S., Uhlenbrook, S., and Ojha, S. An analysis of snow cover changes in the Himalayan region using MODIS snow products and in-situ temperature data. *Climatic Change*, 108:391–400, 2011. DOI: https://doi.org/10.1007/s10584-011-0181-y.

[70] Gurung, D.R., Kulkarni, A.V., Giriraj, A., Aung K.S., and Shrestha, B. Monitoring of seasonal snow cover in Bhutan using remote sensing technique. *Current Science*, 101(10):1364-1370, 2011. DOI: https://www.jstor.org/stable/24079646.

[71] Immerzeel, W.W., Droogers, P., de Jong, S.M., and Bierkens, M.F.P. Large-scale monitoring of snow cover and runoff simulation in Himalayan river basins using remote sensing. *Remote Sensing of Environment*, 113(1): 40-49, 2009. DOI: https://doi.org/10.1016/j.rse.2008.08.010.

[72] Singh, S., Sood, V., Kaur, R., and Prashar, S. An efficient algorithm for detection of seasonal snow cover variations over undulating North Indian Himalayas, India. *Advances in Space Research*, 64(2): 314-327, 2019. DOI: https://doi.org/10.1016/j.asr.2019.04.016.

[73] Xu, J., Grumbine, R.E., Shrestha, A., Eriksson, M., Yang, X., Wang, Y., and Wilkes, A. The Melting Himalayas: Cascading Effects of Climate Change on Water, Biodiversity, and Livelihoods. *Conservation Biology*, 23(3): 520-530, 2009. DOI: https://doi.org/10.1111/j.1523-1739.2009.01237.x.

[74] Shrestha, A.B., and Aryal, R. Climate change in Nepal and its impact on Himalayan glaciers. *Regional Environmental Change*, 11:65–77, 2011. DOI: https://doi.org/10.1007/s10113-010-0174-9.